UCLouvain

epl

École polytechnique de Louvain

CO_2 revalorization using a distillation-crystallisation membrane

A $NaHCO_3$ crystallization study

Author: **Augustin VANDERAA**
Supervisors: **Patricia LUIS ALCONERO, Marie-Charlotte SPARENBERG**
Readers: **Patricia LUIS ALCONERO, Tom LEYSSENS, Yann GARCIA**
Academic year 2022–2023
Master [120] in Chemical and Materials Engineering

Contents

Abstract

Carbon dioxide revalorization is nowadays an important topic because it can help to find solutions to reduce greenhouse gas emissions, which are major contributors to climate change. Indeed, carbon dioxide is the most significant of these gas due to human activities such as the burning of fossil fuels for energy production or transportation and, consequently, is the primary source of the global warming. It is therefore necessary to find a way to reduce carbon dioxide emissions.

A current way to do so is to use an absorption column where carbon dioxide is absorbed into a liquid, often water. This solution does not require a large amount of energy however, the absorbent must be cleaned afterwards and the remaining products have to be stored. This is why carbon dioxide revalorization is even more important in order to find a second life for these products. One of these is the sodium bicarbonate.

Sodium bicarbonate can easily be crystallized and its crystals may find numerous applications, for example in cement or plaster production. In this thesis, the crystallization of sodium bicarbonate thanks to a distillation-crystallization membrane using different parameters will be discussed, and their impacts on the process and the produced crystals will be analyzed.

Chapter 1

Introduction

1.1 Carbon revalorization

Reducing CO_2 emissions is a meaningful way to mitigate the negative impacts of climate change. One way to do this is through CO_2 revalorization, which captures CO_2 emissions and converts them into useful products or materials, rather than releasing them into the atmosphere. This can help to reduce the overall amount of CO_2 in the atmosphere and slow the rate of climate change.

By capturing and reusing CO_2 emissions, it is possible to mitigate their impact on the environment and help to slow the process of climate change. CO_2 revalorization can also create economic value by converting CO_2 into valuable products, which can be sold and used in various applications. This can help to offset the costs of capturing and storing CO_2, and can potentially create new business opportunities and revenue streams.

In addition to its environmental benefits, CO_2 revalorization can also have economic benefits. By capturing and reusing CO_2, we can create value from a waste product that would otherwise be released into the atmosphere. This can help to create new industries and jobs, and potentially generate revenue from the sale of revalorized products.

CO_2 revalorization refers to the process of capturing carbon dioxide emissions and converting them into useful products or materials, rather than simply releasing them into the atmosphere. This can be done through a variety of technologies, including chemical reactions, biotechnology, and physical processes. The goal of CO_2 revalorization is to reduce greenhouse gas emissions and mitigate their negative impact on the environment, while also creating economic value from captured CO_2. Some potential applications for revalorized CO_2 include the production of fuels, plastics, and chemicals, as well as use in enhanced oil recovery and agricultural applications.

Overall, CO_2 revalorization is an important strategy for addressing climate change and creating a more sustainable future.

1.2 Crystallization process

The process of crystallization can be set in motion through different means. Cooling or concentrating the feed solution are two methods that can be employed (see figure 1.1). Once the solubility curve is crossed, an undersaturated solution becomes a saturated solution due to changes in solubility [24].

Once the solubility curve is crossed, two possible ways to initiate crystallization are possible: using seeding or supersaturating even more the solution to cross the spontaneous nucleation curve. It's important to note that the solubility curve is dependent on thermodynamics, while the spontaneous nucleation curve is influenced by kinetics [26]. Based on that, a third way to initiate crystallization involves the introduction of an anti-solvent because it will change the solubility of the solution.

When it comes to membrane crystallization, the type of membrane determines which of these three ways will be followed. For example, by pressurizing and selectively transferring mass, pressure-driven membrane processes such as ultrafiltration, nanofiltration and reverse osmosis concentrate the solution to create supersaturation. Anti-solvent membrane crystallization is a process that uses an anti-solvent to decrease the solubility of the feed solution, allowing for supersaturation to occur and crystals to form on the membrane surface while solid hollow fiber cooling crystallization is used to induce crystallization by lowering the feed temperature through the cooling path. [24]

In this study, a membrane distillation-crystallization is used. In such a membrane, the solvent evaporates through the membrane and allows to increase the concentration of the solution (moving up in figure 1.1).

The vacuum helps to reduce the vapour pressure of the solvent, which makes it easier for the solvent to pass through the membrane. At the same time, the solute is left behind on the concentrated side of the membrane. The resulting permeate stream is purer than the original mixture, while the concentrate stream is more concentrated. [13]

Crystallization can be used in conjunction with VMD to further purify the permeate stream. This can be done by allowing the permeate stream to cool and evaporate, which causes the solute to separate from the solvent and form crystals. The crystals can then be collected and further purified, if necessary, to obtain a highly pure form of the solute. [13]

The advantages of this method are [13]:

- Non-volatile solutes such as macromolecules, colloidal species, and ions have a high likelihood of being rejected.

- The use of lower temperatures and pressures than those typically employed in traditional distillation columns.
- The possibility of efficiently reusing low-grade or waste heat streams, as well as alternative energy sources such as solar, wind, or geothermal.
- Reduction of corrosion problems thanks to the possibility of using plastic equipment

While drawbacks are [13]:

- Lower permeate fluxes and higher energy consumption with respect to pressure-driven membrane processes (MF, UF, NF, RO).
- Only certain types of polymers provide the necessary chemical resistance and operational stability.
- Although the price of membranes is decreasing, commercial modules remain relatively expensive.

Supersaturation is the driving force for crystallization and is a prerequisite before a solid phase will appear in a saturated solution [2].

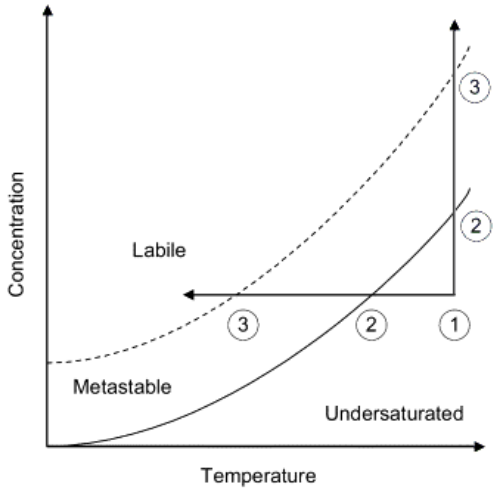

Figure 1.1: At point 1 the system is undersaturated and the concentration of dissolved solute is below the solubility curve defined by equation 2.1. As the system cools or evaporates it becomes saturated at point 2 but remains as a metastable liquid phase until the metastable zone is crossed at point 3, where crystals of the solute will spontaneously form. This process is called nucleation. [2]

When supersaturation is achieved, the nucleation can occur rapidly, aided by the presence of a membrane that serves as a site for nucleation [1]. The membrane's distinct properties facilitate the process, making it possible for the substance to transition to a more stable state [1].

It is crucial to acknowledge that the occurrence of polarization phenomena produces dissimilar circumstances at the membrane as compared to the bulk. Consequently, this results in a decrease in temperature and an increase in concentration at the membrane surface. This, in turn, fosters the process of crystallization on the membrane instead of in the bulk solution. [13] When nucleation occurs on the membrane, crystal detachment via flow shear stress is usually desired in order to conduct the nuclei to a separate crystallizer for further growth. [10] The purpose of this is to minimize the possibility of membrane scaling and blockage [17].

1.3 Sodium bicarbonate crystallization

The current most process to produce $NaHCO_3$ crystals is through precipitation in an industrial bubble column crystallizer. The methodology presented in Figure 1.2 consists of three primary phases[9].

1. Feed solution preparation: The process of obtaining a qualified feed solution involves dissolving raw materials such as light soda ash and defective crude heavy soda ash in filtrate that has been recycled from the $NaHCO_3$ filtering process. The resulting solution is then passed through a clarifying device to eliminate impurities before being filtered through a PE membrane to obtain the desired final product. [9]

2. Carbonation crystallization: At the pinnacle of the tower, a highly concentrated solution of Na_2CO_3 is introduced and allowed to flow in the opposite direction of purified kiln gas. The gas consists of approximately 38-40% CO_2 and is generated by the breakdown of $CaCO_3$ at elevated temperatures. [9] The process of separating CO_2 gas and dust CaO solid can be efficiently achieved through the use of a cyclone separator, seawater washing, and electrostatic precipitation, which effectively remove fine particles. Additionally, a slurry of $NaHCO_3$ crystals is produced in the tower and can be conveniently extracted from the bottom.

3. Dryness of the products: The slurry containing $NaHCO_3$ is subjected to a filtration process and then dried in a heated air-swept dryer. Afterwards, fresh soda ash is dissolved in the resulting filtrate. [9]

However, this process may present some drawbacks and the use of a membrane to perform the crystallization could be a great alternative. Indeed, it presents the

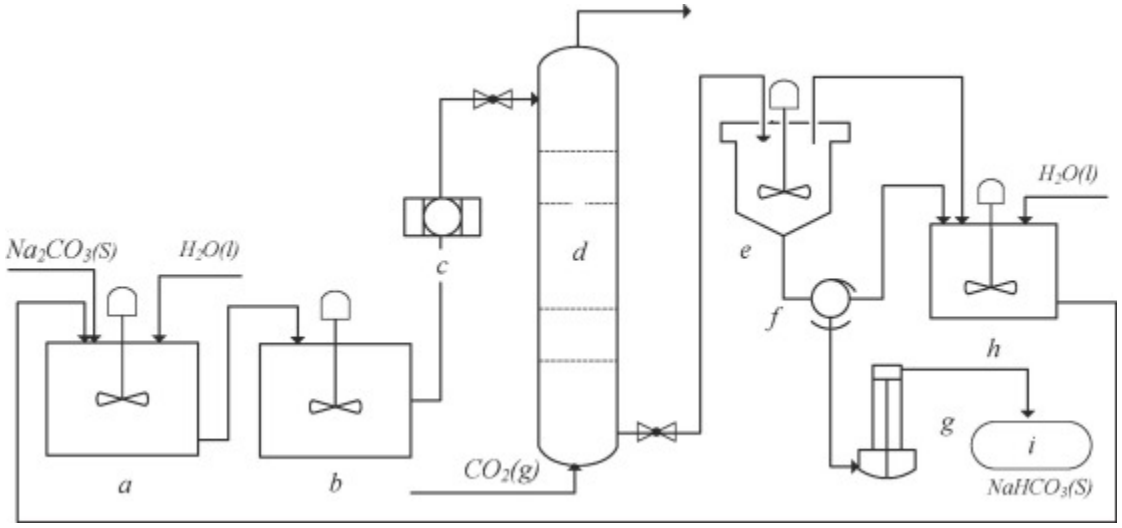

Figure 1.2: Process flow diagram of sodium bicarbonate: (a) Alkali barrel, (b) clarifying tank, (c) PE filter, (d) carbonation tower, (e) thickener, (f) centrifuge, (g) dryer, (h) liquor barrel, and (i) product [9]

following advantages compared to a column: Amongst other advantages, membranes can often be run in continuous mode, allowing for a consistent and steady separation. This can be advantageous for large-scale production and maintaining product quality. It also can provide high purity separation due to their selective permeability, unwanted impurities and smaller molecules can be effectively removed, leading to a purer product. Membrane processes typically operate at lower temperatures and pressures compared to traditional column-based processes, leading to reduced energy consumption and potential cost savings. They are generally more easily scalable than column processes, allowing for smoother transitions from laboratory-scale experiments to industrial-scale production and they often require smaller amounts of solvents compared to column processes, resulting in less waste generation and a more environmentally friendly approach. Properly designed membrane systems can exhibit reduced fouling tendencies, leading to longer operational lifetimes and less downtime for maintenance. Such processes can furthermore enable selective crystallization by allowing only certain components to pass through, leading to the formation of specific crystalline products. It often requires less mixing, which can be beneficial for delicate crystallization processes where excessive agitation could lead to unwanted crystal damage. And finally, it generally requires less physical space compared to traditional column-based setups, which can be advantageous in situations where space is limited.

Different types of membranes can be employed for various separation tasks, making the process adaptable to different feed compositions and separation re-

quirements. This thesis will focus on the crystallization of $NaHCO_3$ thanks to a distillation-crystallization membrane and try to determine which are the best parameters to perform this crystallization.

The structure of the study will be the following:

First, the materials and methods used to perform the study will be introduced. The results will then be presented and afterwards, a discussion will be made. Finally, a conclusion will be done at the end.

[24]

Chapter 2

Materials and methods

As said previously, the crystallization of the $NaHCO_3$ is performed thanks to a membrane contactors, and more precisely, a distillation-crystallisation membrane. Several configurations of these membranes exist but only the vacuum membrane distillation will be analyzed in this thesis. The other configurations analysis is let to be performed in further work studies.

In this chapter, the setup used to perform the crystallisation of $NaHCO_3$ will be first described as well as the different materials and devices used.

Afterwards, the methods used to prepare and analyze the different samples will be explained.

2.1 Materials

The setup is shown in figure 2.1. It is composed of:

- The distillation-crystallisation membrane
- A crystallization tank
- A rotating device
- A circulation pump
- A two heater devices
- A condensation column
- A cooler device
- A vacuum pump
- A permeate tank

The crystallization tank is where the crystallization is supposed to take place. The rotating device is placed into the crystallization tank in order to keep its content continually perfectly mixed. Its rotation speed can be tuned. One of the heaters is used to keep the crystallization tank at the desired crystallization temperature while the other heater is present to heat up the solution before it goes through the membrane where it partially evaporates to the condensation column. The condensation column is maintained under a level of vacuum that can be tuned thanks to a vacuum pump. It is also kept at -2.5 [°C] with the cooler device in order to condensate the liquid that has evaporated through the membrane. This condensed liquid is recovered in a permeate tank. Finally, a circulation pump allows the solution to flow in the system at a tunable flow rate.

The solutions are prepared with pure $NaHCO_3$ found in the commerce (see appendix B) and ultra-pure water.

The membrane characteristics are given in the appendix A.

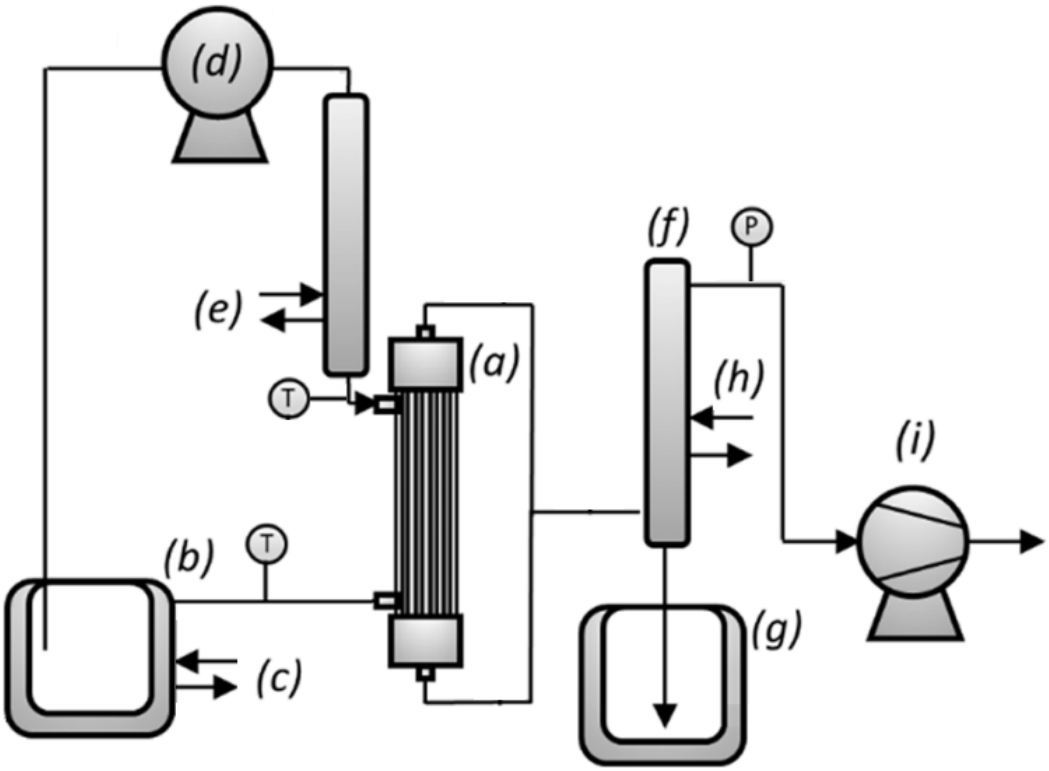

Figure 2.1: The setup used for the crystallisation of $NaHCO_3$ including (a) a distillation-crystallisation membrane, (b) a crystallization tank, (c) and (e) two heater devices, (d) a circulation pump, (f) a condensation column, (g) a permeate tank, (h) cooler and (i) vacuum pump.

2.2 Methods

2.2.1 Tested parameters

The tested parameters are the followings:

- The flow rate in the system
- The rotation speed of the mixer in the crystallization body
- The temperature at the inlet of the membrane
- The level of vacuum at the outer side of the membrane

Since every experiment takes several hours, it was difficult to perform more than two per tested parameters due to time considerations. However, some experiments were done more times if a problem or anomaly occurred and if an odd result was observed.

2.2.2 Reference experiment

A few experiments have been performed previously to determine the range in which the parameters would have been possible to study. Indeed some limitations, materials as well has time, had an impact on this range.

From these previous experiments, a reference one has been decided since it was showing good results. This reference experiment is:

- Flow rate [ml/min]: 300
- Rotation speed [turns/min]: 72
- Inlet temperature [°C]: 40
- Vacuum [mbar]: 15

2.2.3 Experiments choices

It is important to note that only one parameter at a time is changed from the reference experiment to study properly its impact.

If we refer to the specification of the membrane A, wetting of the membrane occurs when the flow rate of the solution through the membrane is about 500 [ml/min]. Since such a phenomenon reduces the mass transfer in the membrane [21], it is essential to avoid going to this value. This is why the maximum flow rate was set to 400 [ml/min]. The second and lower limit of the flow rate was set by the pump. Indeed, it can hardly go below a flow rate of 100 [ml/min] which is thus the lower limit decided.

The minimum rotation speed was also decided by material issues. The rotating device had difficulties keeping a constant rotation speed below 72 [turns/min] and had the tendency to jerk beneath this value. The top limit value is determined by the fact that vortexes should be avoided in the crystallization body since it would directly impact the residence time of the particles. This defines the maximum value of the rotation speed since a vortex started to appear above 131 [turns/min].

Again, the specification of the membrane gives us the maximum temperature allowed in it without inducing damage of 40[°C]. The minimum temperature was decided by the time needed to start the crystallization. At a temperature of 30[°C], more than 9 hours were needed. A minimum temperature of 35[°C] was thus

chosen in order to allow crystallization in a reasonable time. Note that it was not possible to let the system runs during the night or without surveillance since the vessel collecting the condensed water had to be regularly emptied, samples had to be taken when crystallization occurs, and finally, the experiment had to be stopped before crystallization started to occur inside the membrane which would have damaged it.

The maximum level of the vacuum of 40 [mbar] was also decided by time and efficiency considerations: the higher the vacuum, the lower the evaporation rate through the membrane. Also, the vacuum pump was not able to go below 15 [mbar] which is thus the lower limit of this parameter.

Finally, a value was taken inside each of those ranges in order to spot a trend in the impacts of the parameters.

To summarize, the following experiments were performed:

- Flow rate [ml/min]: 100, 300 and 400
- Rotation speed [turns/min]: 72, 98 and 131
- Inlet temperature [°C]: 35, 37.5 and 40
- Vacuum [mbar]: 15, 30 and 40

2.2.4 Experiments methodology

Each experiment has been conducted as follows:

A saturated solution is prepared for 1.4 [l] of pure water. Depending on the experiment temperature, the mass of $NaHCO_3$ that has to be added differs and follows the equation 2.1:

$$m_{NaHCO_3} = V\,(0.006\,T^2 + 1.2195\,T + 68.946) \tag{2.1}$$

This equation gives the mass of $NaHCO_3$ in [g] for a given volume of solvent V in [l] and the temperature T is in [°C] and has been determined experimentally. In order to be sure that saturation is achieved, ten more grams were added each time.

The solution was covered right after the addition of $NaHCO_3$ with a latex glove to keep the degassing CO_2 in contact with the solution. Doing so, the equilibrium was not shifted and the pressure was kept atmospheric.

Finally, the vessel containing the solution was mixed thanks to a magnetic stirrer added beforehand and heated with a water bath to be heated homogeneously. The water bath was heated one degree above the temperature of the conducted experiments, again in order to ensure the saturation of the solution. Since it was impossible to heat and mix the solution simultaneously, the vessel carrying it was

transferred from the bath to the stirred multiple times (typically three) and then left to rest in the bath for the night.

Before introducing the solution into the system, this one was clean always in the same way. Namely, by introducing pure water and making it circulates at a flow rate of 300 [ml/min]. Also, during this cleaning, the heaters and the cooler were started and brought to their experiment temperature.

Once the cleaning was achieved, the cleaning water was removed and, for each experiment, 1.2 [kg] of the solution was taken and placed in the preheated crystallisation tank paying attention that the remaining $NaCO_3$ that had not dissolved does not drop into it.

The circulation pump was then set at the experiment flow rate and, once the solution had entirely filled the system, the vacuum pump was started and also set at its experiment specification.

During the experiment, the water collected in the condensation column had to be removed once because the collecting bottle had a limited capacity. Indeed, a bigger bottle presents risks of implosion due to low pressure. While the condensed water was removed, the pressure outside the membrane had to be set back to atmospheric pressure. At the end of the experiment, the condensed water was again removed. The moments and the quantities of water have been recorded to roughly estimate if there was a difference in flux between the beginning and the end of the experiment.

Once the first crystals appeared, a 10 [ml] sample was taken and filtered. To note that this first observation was made with the naked eye. The possibility of using a turbidity probe has been explored but was not conclusive because the crystallization tank was not high enough. Two other samples were also taken five and ten minutes after the first apparition. It was not possible to take more samples because the growing crystals could have obstructed the membrane which could damage it and made the experimentation fail.

Right after the third sampling, all the remaining solution with crystals was collected and filtered.

After the experiments, the system was again cleaned several times with pure water at a flow rate of 300 [ml/min].

2.2.5 Studied parameters

The main parameters that wanted to be studied are the induction time, the transfer coefficient, the size and shape of the crystals and, finally, their yield.

The growth rate of the crystals was considered at first for this study by analysing the images obtained with the SEM from the different samples at different times of the crystallization. But the first experiments showed very entangled crystals which

makes impossible the use of such techniques since it requires to be able to observe both ends of the crystals. This was therefore abandoned.

Induction Time

The induction time is defined here as the time needed to observe the first crystals.

The use of a turbidity probe was considered to measure more precisely this induction time but it was not possible to properly set it up. Indeed, the probe needed at least ten centimetres of liquid to measure correctly the turbidity of the solution. It was thus decided to measure it with the naked eye even if this will undeniably lead to larger inaccuracies.

Few studies were performed about induction times [24]. However, one can expect the evaporation rate [5] as well as the flow rate [19] to have a significant impact. Furthermore, the type of membrane should also have an influence since studies showed that high surface porosity and pore size leads to a reduction of nucleation time [4].

Since the same membrane was used for all the experimentation, the analysis of the impact of the type of membrane on the crystallization of $NaHCO_3$ is left for further studies.

Transfer coefficient

From the induction time (t) and knowing the initial and final mass of the solution (M_i and M_f), it is possible to compute the flux through the membrane:

$$J = \frac{M_i - M_f}{t \cdot A} \tag{2.2}$$

Where A is the membrane area (18 [m^2]).

The flux is also given by:

$$J = K_{ov} \left(p_f^* \, a_f - p_p \right) \tag{2.3}$$

Where K_{ov} is the overall mass transfer coefficient, p is the water vapour pressure and a is the water activity. Subscripts denote the feed (f) and the permeate (p).

The water vapour pressure of the feed is given in [mm_{Hg}] by:

$$p^* = 10^{8.07131 - \frac{1730.63}{233.426 + T}} \tag{2.4}$$

At the feed, the water vapour pressures are summarized, after conversion (1 [mm_{Hg}] = 133.32 [Pa]), in the table 2.1. At the permeate side, the water vapour pressure is equal to the pressure applied.

Temperature [°C]	35	37.5	40
Water vapour pressure [Pa]	5609	6432	7358

Table 2.1: Water vapour pressure of the feed in function of the temperature

The water activity can be determined tanks to the molality and to a table found in the literature (see figure 2.2). This table gives the activity coefficient for a temperature of 20 [°C] but unfortunately, the information was not found for other temperatures. These values will thus be used in this study. The water is assumed

m / mol·kg^{-1}	$\gamma_\pm$	ϕ	a_w	G^{ex} / J·kg^{-1}	m / mol·kg^{-1}	$\gamma_\pm$	ϕ	a_w	G^{ex} / J·kg^{-1}
0.001	0.965	0.989	0.99996	0	0.080	0.795	0.937	0.99730	−66
0.002	0.952	0.984	0.99993	0	0.090	0.788	0.935	0.99697	−78
0.003	0.943	0.981	0.99989	−1	0.100	0.780	0.933	0.99664	−90
0.004	0.935	0.979	0.99986	−1	0.200	0.731	0.919	0.99340	−230
0.005	0.928	0.976	0.99982	−1	0.300	0.699	0.909	0.99022	−397
0.006	0.922	0.975	0.99979	−2	0.400	0.674	0.900	0.98711	−583
0.007	0.917	0.973	0.99976	−2	0.500	0.653	0.891	0.98407	−787
0.008	0.912	0.971	0.99972	−3	0.600	0.634	0.883	0.98110	−1005
0.009	0.908	0.970	0.99969	−3	0.700	0.617	0.874	0.97819	−1238
0.010	0.904	0.969	0.99965	−3	0.800	0.602	0.866	0.97534	−1483
0.020	0.873	0.959	0.99930	−9	0.900	0.587	0.858	0.97256	−1741
0.030	0.852	0.953	0.99897	−17	1.000	0.574	0.850	0.96984	−2011
0.040	0.837	0.949	0.99863	−25	1.223	0.546	0.832	0.96400	−2653
0.050	0.824	0.945	0.99830	−34	1.250	0.543	0.830	0.96331	−2735
0.060	0.813	0.942	0.99797	−44	1.300	0.537	0.826	0.96204	−2887
0.070	0.804	0.939	0.99763	−55					

Figure 2.2: Mean ionic activity coefficients γ_+, osmotic coefficients ϕ, activities of water a_w and excess Gibbs energies G^{ex} for aqueous $NaHCO_3$, at selected molalities m at 298.15 K [22]

pure at the permeate side and thus, its water activity is equal to 1.

The molality is the number of moles of solute per mass of solvent. From equation 2.1 the molality is given by:

$$m = \frac{m_{NaHCO_3}/M_{NaHCO_3}}{V \cdot \rho} \tag{2.5}$$

Where M_{NaHCO_3}, the molar weight of the solute, is equal to 84 [g/mol] and V and ρ are respectively the volume and the density of the solvent.

The values of the molality and the water activity for the three temperatures are summarized in the table 2.2

[22]

Temperature [°C]	35	37.5	40
Molality [mol/kg]	1.321	1.368	1.416
Water activity [/]	0.962	0.96	0.959

Table 2.2: Molality and water activity of the solutions in function of the temperature

Size and shape

The physical characteristics of crystals are determined by their crystal habit and polymorphism. Crystal habit pertains to the external shape of the crystal, while polymorphism refers to the variation in internal structure and habit of identical molecule crystals [24]. It is possible for a single compound to exhibit different crystal habits without undergoing any polymorphic changes [7].

The extent to which a solution is supersaturated plays a crucial role in determining the specific shape of the resulting crystals. The higher the degree of supersaturation, the greater the likelihood that the crystals will exhibit distinct and well-defined morphologies, which can vary widely depending on the chemical composition and physical properties of the solute and solvent. This phenomenon is of significant interest to researchers across a range of fields, as it has important implications for the development of new materials, drug delivery systems, and other applications [11].

Supersaturation may result from several conditions [8]:

- Cooling an ordinary salt solution or heating an unusual salt solution can lead to supersaturation.
- The concentration of the solution increases as water evaporates. After a certain period, it becomes saturated and then supersaturated.
- When a soluble salt with a common ion or produces a sparingly soluble salt is added to a solution of another salt, the solubility limit may be exceeded because the ionic product becomes more significant than the solubility constant.
- The mixing of saturated or near-saturated solutions may result in supersaturation due to temperature changes.
- Carbon dioxide equilibrium in cooling water tower with atmospheric air

The supersaturation can be computed with the following equation:

$$\sigma = 1 - \frac{M_{solvent,f}}{M_{solvent,i}} = 1 - \frac{M_f \cdot (1 - C_{Na_2CO_3} - C_{NaHCO_3})}{M_i \cdot (1 - C_{NaHCO_3,sat})} \tag{2.6}$$

With $M_{solvent,f}$ the final mass of solvent [kg], $M_{solvent,i}$ the initial mass of solvent [kg], M_f the final mass of solution, $C_{Na_2CO_3}$ the final concentration of sodium carbonate, C_{NaHCO_3} the final concentration of sodium bicarbonate, M_i the initial mass of solution, and $C_{NaHCO_3,sat}$ the saturation concentration of sodium bicarbonate.

The final concentrations of sodium carbonate and sodium bicarbonate are determined through titration while the saturation concentration of sodium bicarbonate is known with the formula 2.1.

Based on the supersaturation, a crystal morphology is expected as shown in figure 2.3.

The size distribution computation of the crystals was performed through granulometry analysis. Distillation-crystallization membranes usually showed narrower size distribution than conventional crystallization processes [24].

It is expected to have an increasing coefficient of variation and mean diameter if the time of crystallization increases [24]. However, some studies have observed a decrease in the mean diameter with time due to a secondary nucleation [20] [4]. It will not really be possible to analyze this effect here because all samples were taken at the same time. Only the reference experiment was left once during the night to maximize crystallization.

The membrane composition could also lead to higher uniformity [15] [18] but this will not be explored in this study.

Furthermore, some studies showed that a low flow rate could increase the mean diameter of the crystals [23] [19]. The reason behind this can be attributed to either the prolonged residence time in the crystallizer which allows more time for the crystals to grow, or either to the resistance integration of the crystals into the crystal lattice [24]. Nevertheless, some other studies showed that a higher flow rate could also increase the mean diameter thanks to particle diffusion limitation [12] [19].

The feed temperature is another parameter that can have an impact. For this parameter too, studies show contradictory results depending on the membrane used: upon increasing the feed temperatures, it was observed that there was a corresponding reduction in both the coefficient of variation and mean diameters for DCMD [14] but a decreasing coefficient of variation for PVDF membrane [19]. Some other membranes do not show any trend for increasing temperature.

A last possibility to influence the size distribution of the crystals is to perform seeding. Indeed, by doing so, small crystals are less likely to appear and the coefficient of variation decrease.

Optimizing each crystallization system individually is, therefore, necessary as variables can affect crystal size distribution differently depending on the salt and process conditions [23].

Crystal yield

Designing a crystallization process with a high crystal yield is crucial for its economic viability [24].

The crystal yield of processes using a distillation-crystallisation membrane is usually low compared to the conventional crystallization yield of around 80% This could be explained by the scale of the crystallization processes but this has still to be studied [24].

Unfortunately, no common formula seems to be accepted to compute the crystal yield [24].

However, the theoretical crystal yield will be here computed as follows [16] [3]:

$$Y_T = w \cdot R \frac{C_1 - C_2 (1 - V)}{1 - C_2 (R - 1)} \tag{2.7}$$

With C_1 [kg anhydrous salt/kg solvent] the initial solution concentration, C_2 [kg anhydrous salt/kg solvent] the final solution concentration, w the initial mass of solvent [kg], R the ratio of molar masses hydrated crystal and anhydrous crystals, and V [kg per kg of original solvent] the solvent lost by evaporation [24].

The initial concentration and the initial mass of the solvent are known using the formula 2.1. The final solution concentration is determined by titration. The ratio of molar masses of hydrated crystals and anhydrous crystals is determined thanks to X-ray diffraction by doing a comparison between the peaks of the different existing phases. And finally, the solvent lost by evaporation is known thanks to a mass balance during the crystallization.

Based on the theoretical crystal yield, the percent yield Y_p can be determined:

$$Y_p = \frac{w_p}{Y_T} \tag{2.8}$$

with w_p the product weight.

Studies showed that the crystallization yield increases with an increasing feed temperature [6]. Seeding should as well allow to increase the yield [27] but this was not performed in this study.

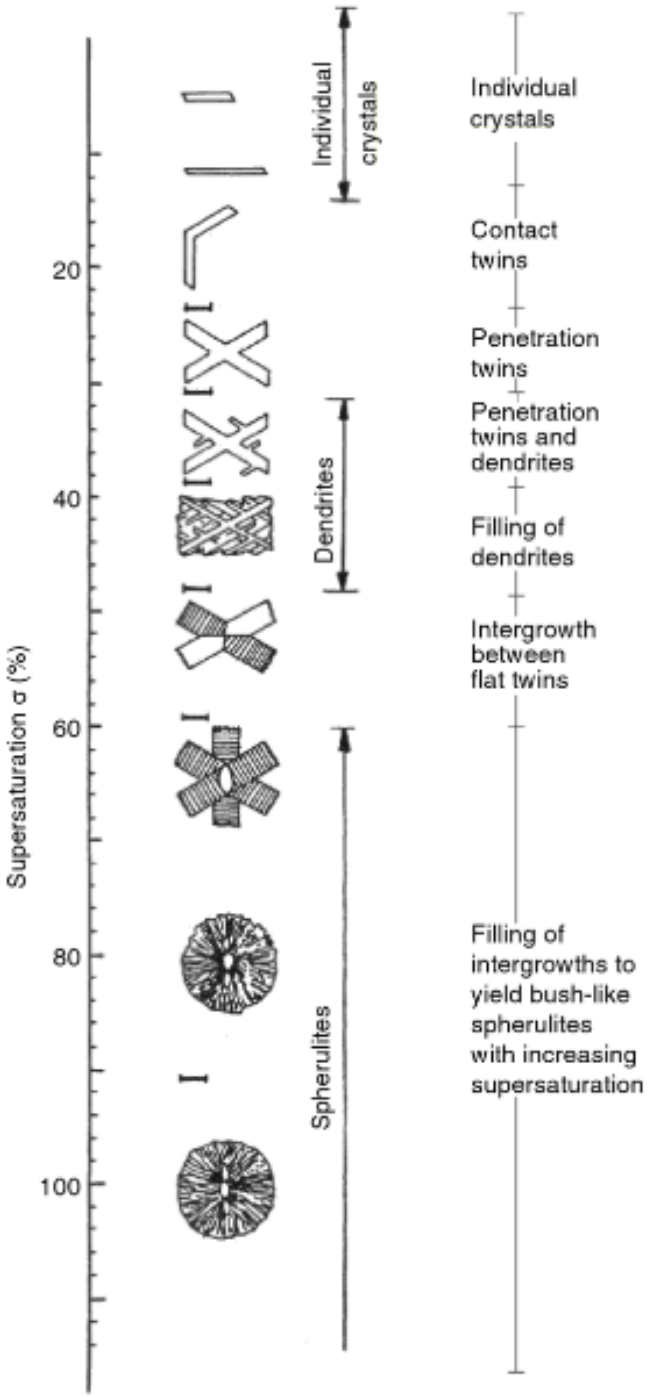

Figure 2.3: Schematic illustration of change in morphology of $NaHCO_3$ crystals with supersaturations [3]

Chapter 3

Results

In this chapter, the results obtained will be presented without interpretations that will be done in a further chapter.

As a reminder, the main parameters that wanted to be studied are the induction time, the transfer coefficient, the size and shape of the crystals and, finally, their yield.

3.1 Induction time

The induction times obtained for the different experiments are shown in the figures 3.1, 3.2, 3.3 and 3.4.

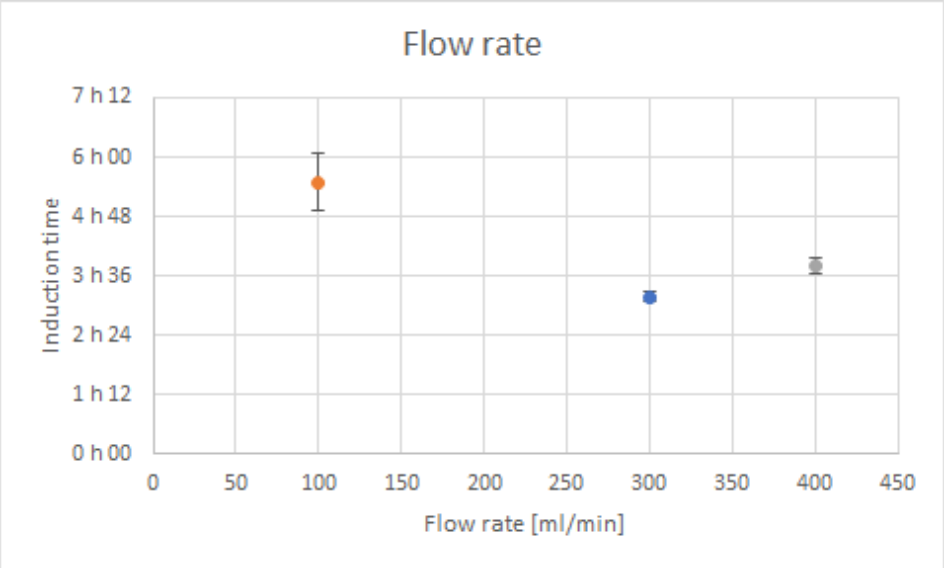

Figure 3.1: Induction time in function of the flow rate in the system

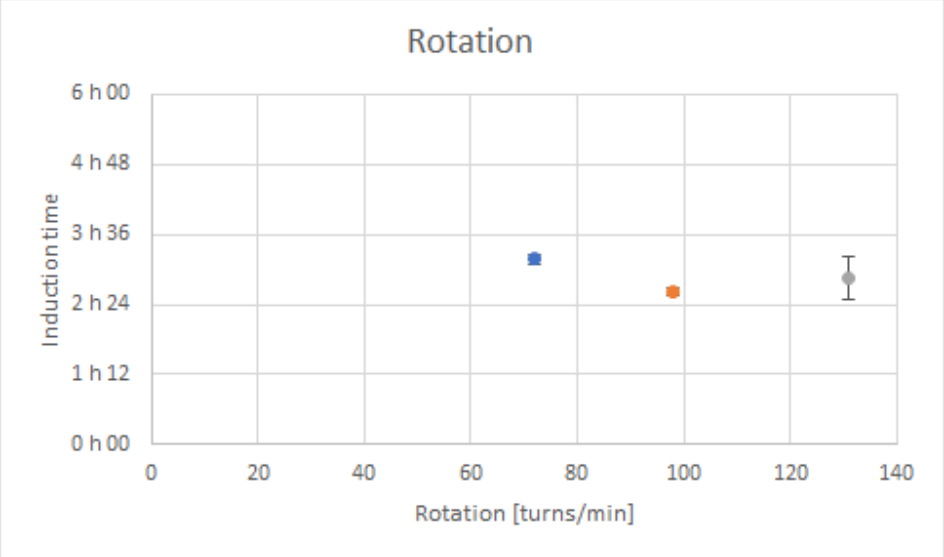

Figure 3.2: Induction time in function of the rotation speed of the mixer in the crystallization body

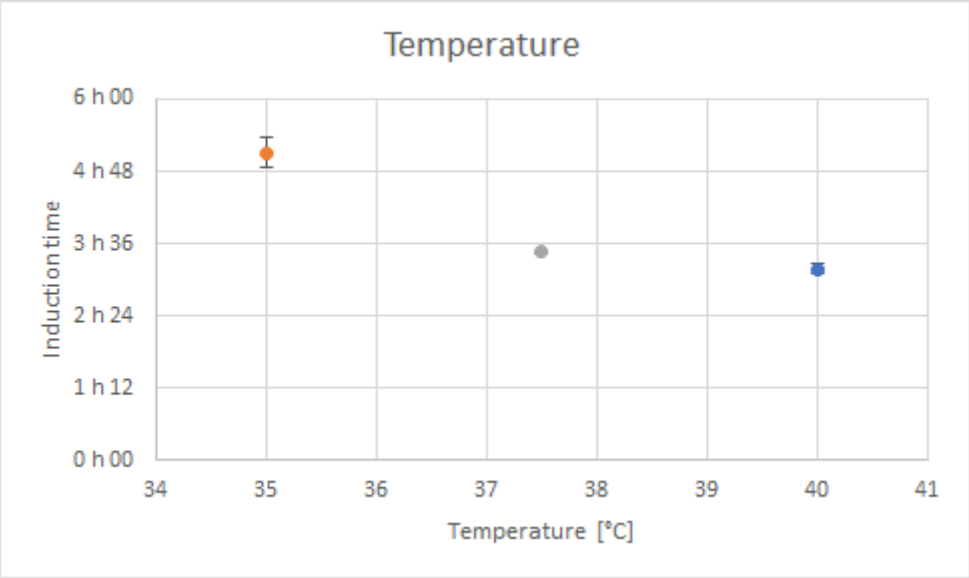

Figure 3.3: Induction time in function of the temperature at the membrane inlet

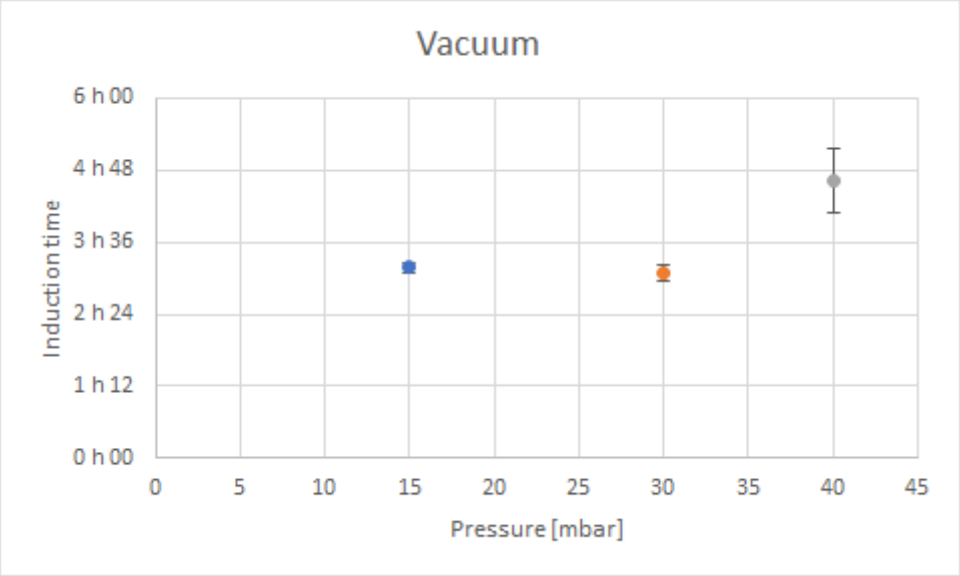

Figure 3.4: Induction time in function of the level of vacuum at the outer side of the membrane

3.2 Transfer coefficient

The flux through the membrane obtained for the different experiments are shown in the figures 3.5, 3.6, 3.7 and 3.8.

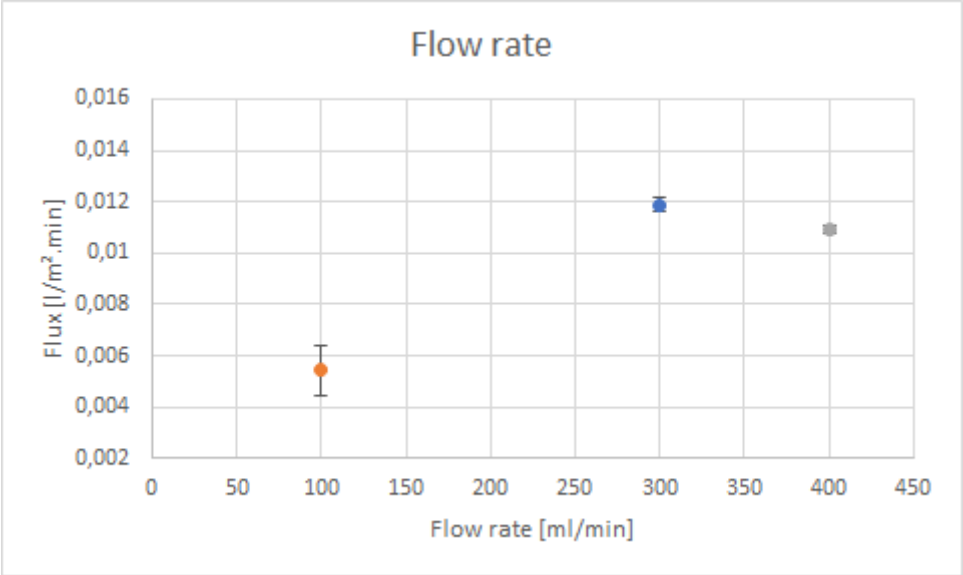

Figure 3.5: Flux through the membrane in function of the flow rate in the system

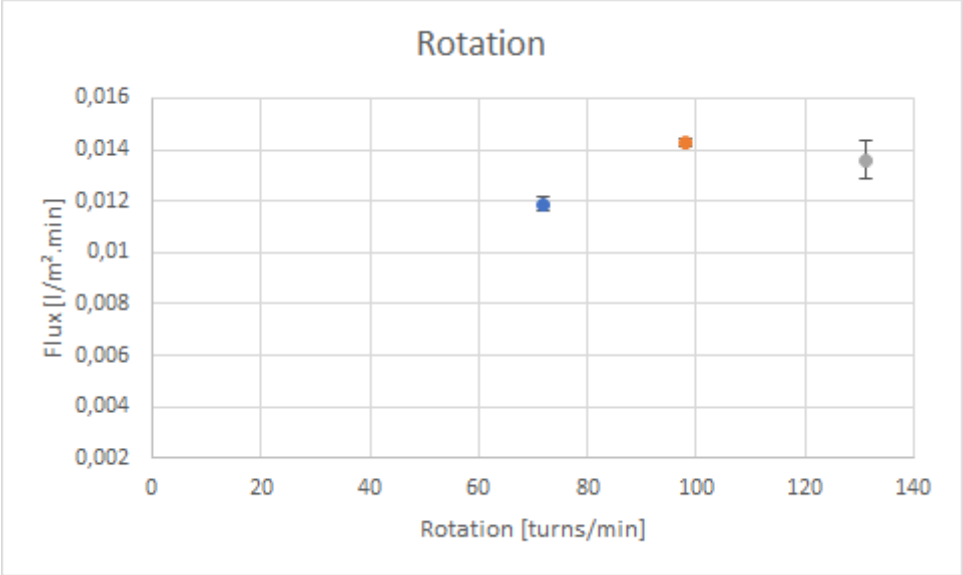

Figure 3.6: Flux through the membrane in function of the rotation speed of the mixer in the crystallization body

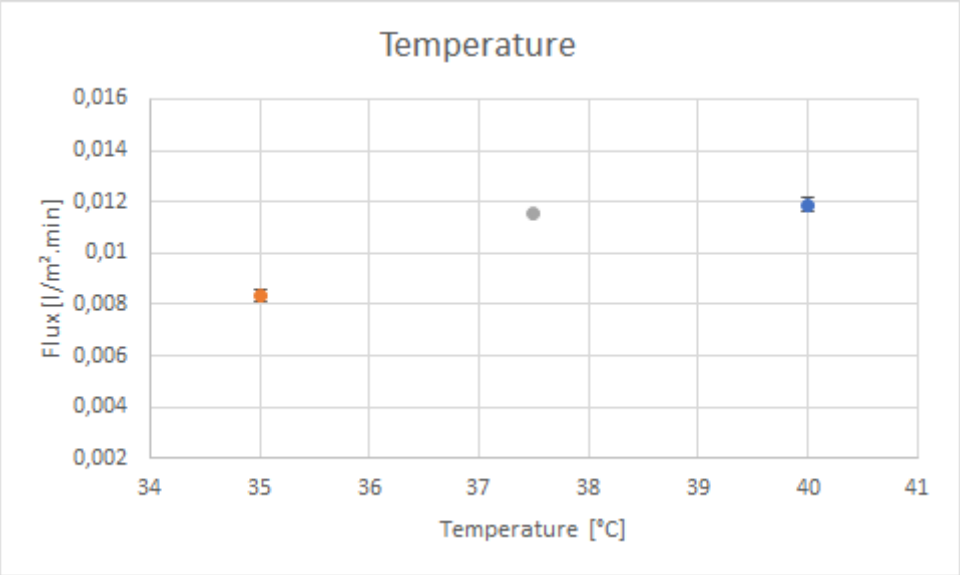

Figure 3.7: Flux through the membrane in function of the temperature at the membrane inlet

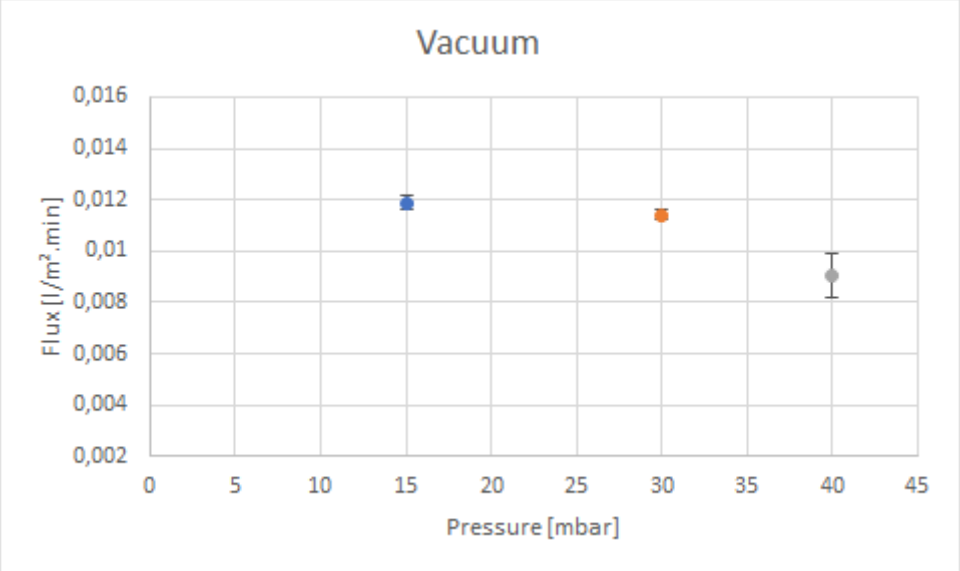

Figure 3.8: Flux through the membrane in function of the level of vacuum at the outer side of the membrane

The overall transfer coefficients obtained for the different experiments are shown in the figures 3.9, 3.10, 3.11 and 3.12.

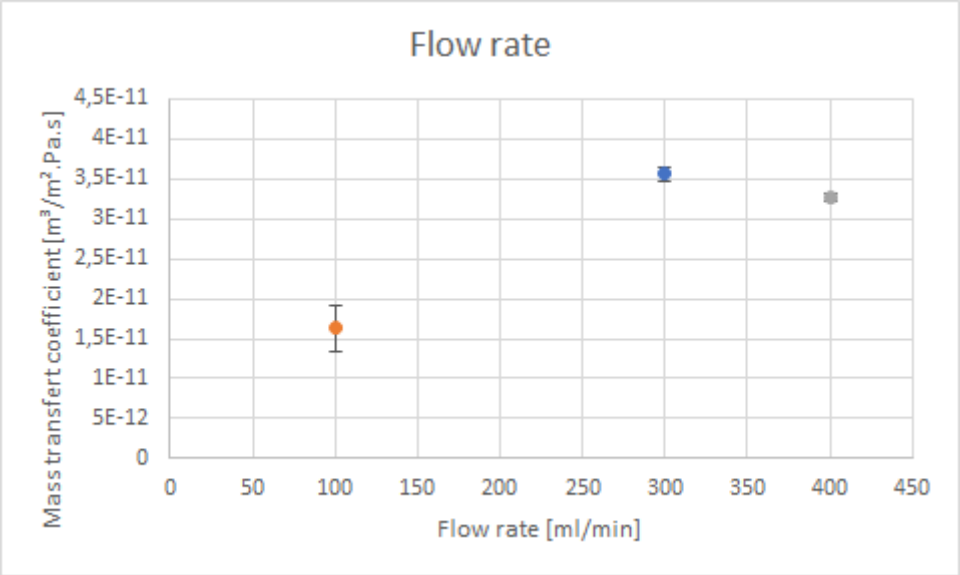

Figure 3.9: Overall transfer coefficients in function of the flow rate in the system

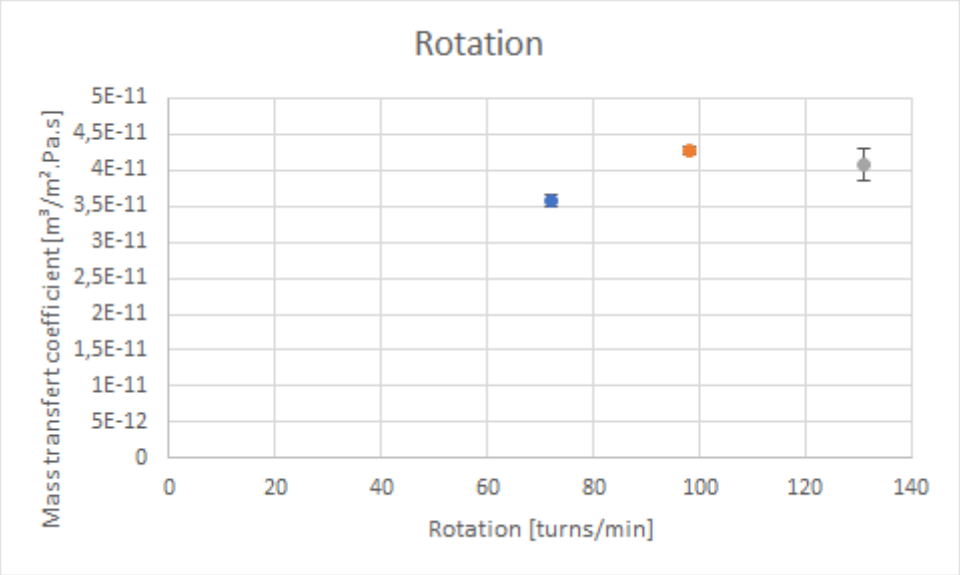

Figure 3.10: Overall transfer coefficients in function of the rotation speed of the mixer in the crystallization body

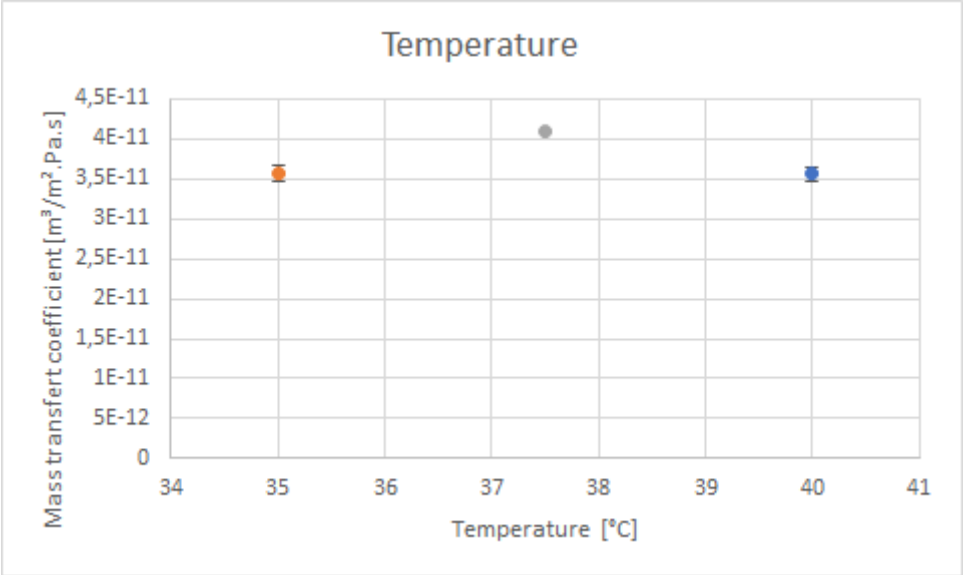

Figure 3.11: Overall transfer coefficients in function of the temperature at the membrane inlet

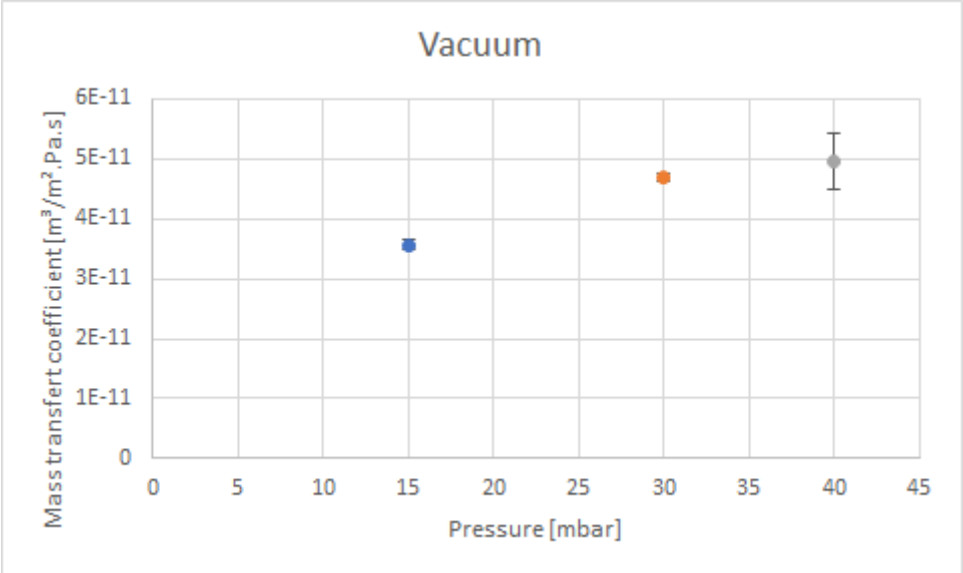

Figure 3.12: Overall transfer coefficients in function of the level of vacuum at the outer side of the membrane

3.3 Size and shape

The supersaturations obtained for the different experiments are shown in the figures 3.13, 3.14, 3.15 and 3.16.

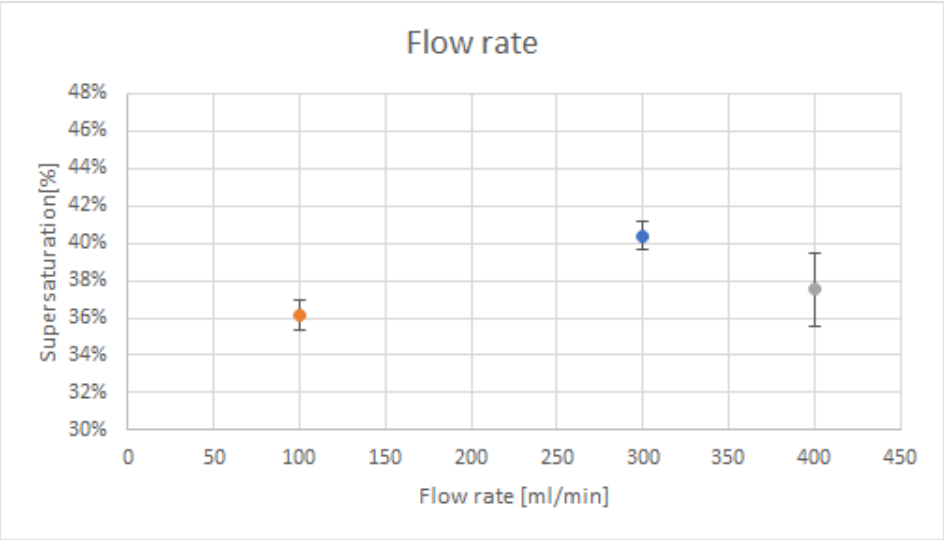

Figure 3.13: Supersaturation in function of the flow rate in the system

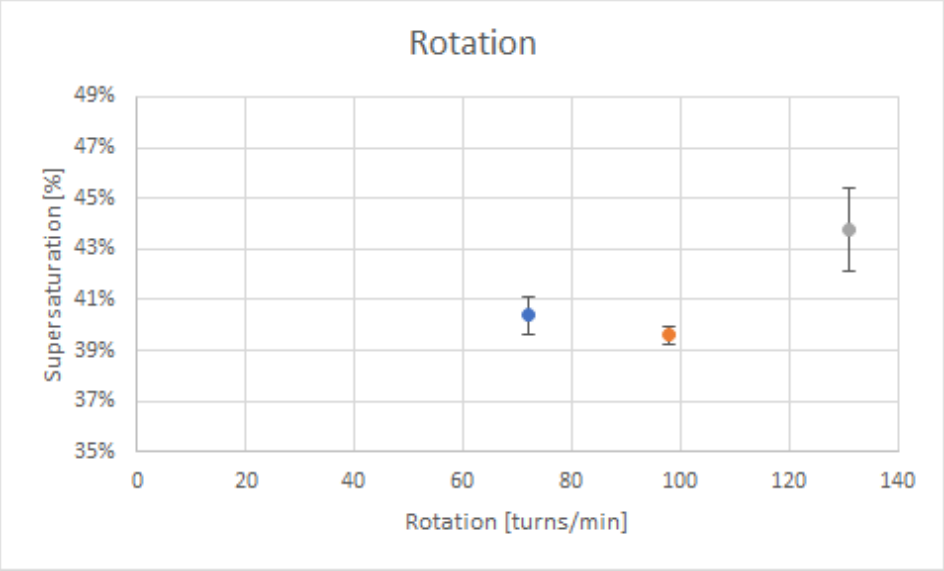

Figure 3.14: Supersaturation in function of the rotation speed of the mixer in the crystallization body

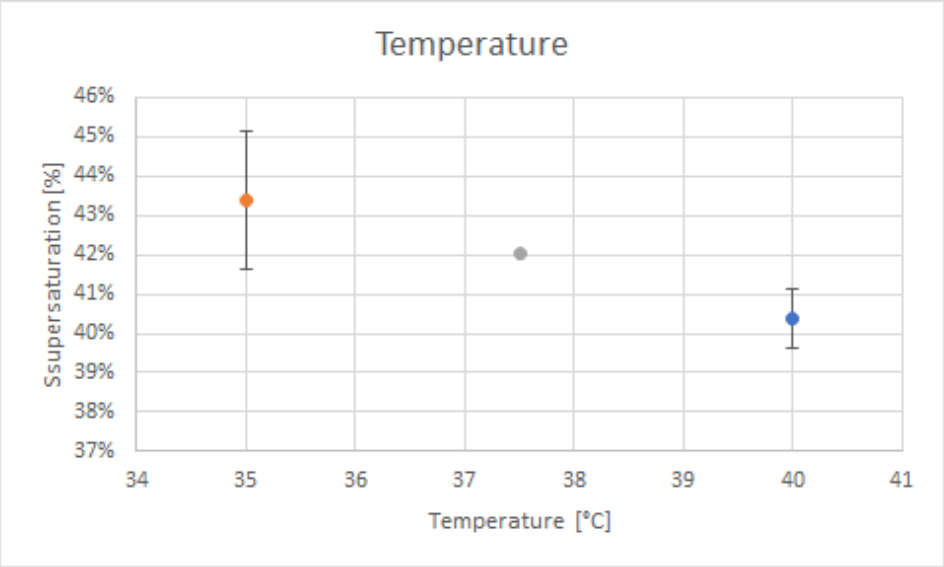

Figure 3.15: Supersaturation in function of the temperature at the membrane inlet

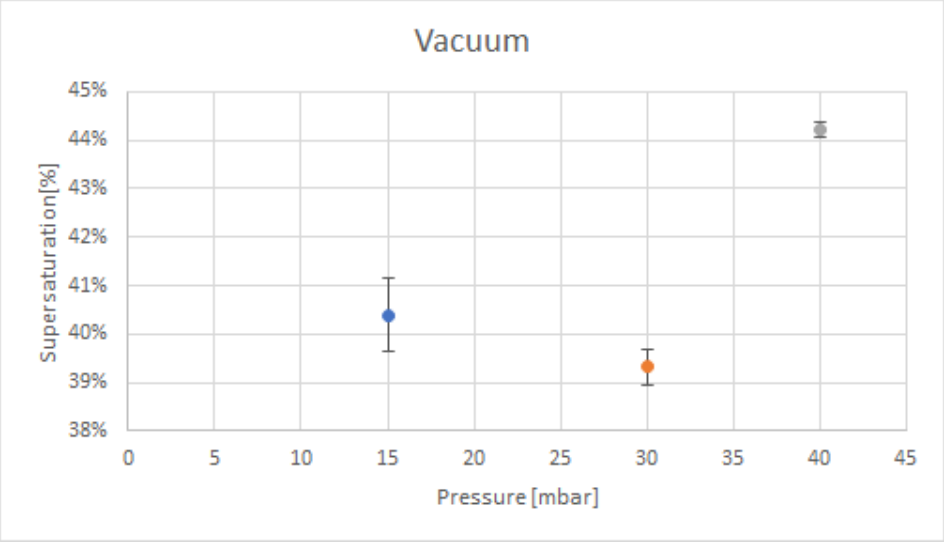

Figure 3.16: Supersaturation in function of the level of vacuum at the outer side of the membrane

Pictures of the crystals obtained with SEM are shown in the figures 3.17, 3.19, 3.18 and 3.20. The times 0 are the samples taken when crystallization was first observed, times 1 are the samples taken five minutes after that and times 2 are those taken ten minutes after the first observed crystallization.

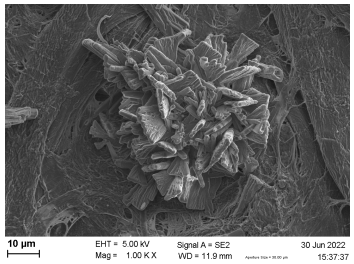

(a) 100 [ml/min], Time 0

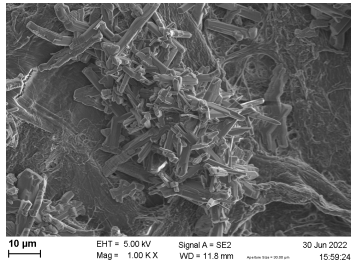

(b) 100 [ml/min], Time 1

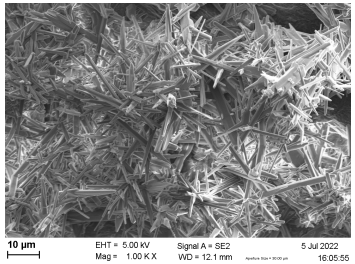

(c) 100 [ml/min], Time 2

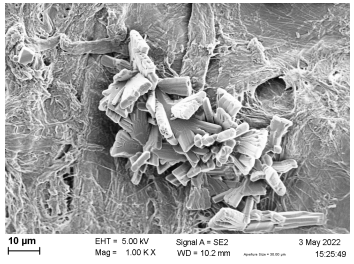

(d) 300 [ml/min], Time 0

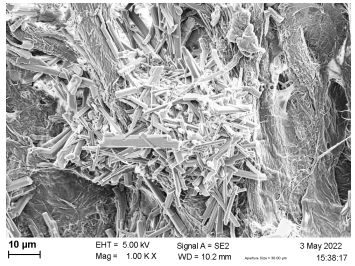

(e) 300 [ml/min], Time 1

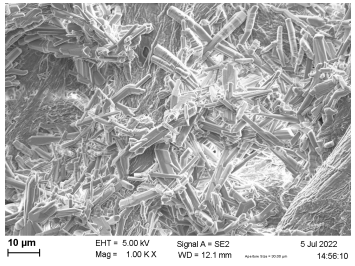

(f) 300 [ml/min], Time 2

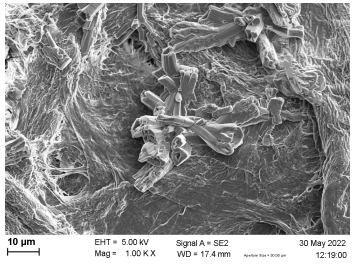

(g) 400 [ml/min], Time 0

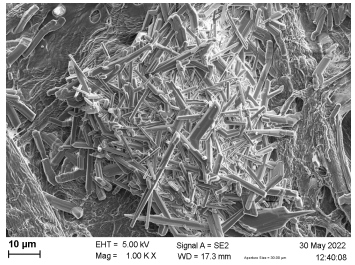

(h) 400 [ml/min], Time 1

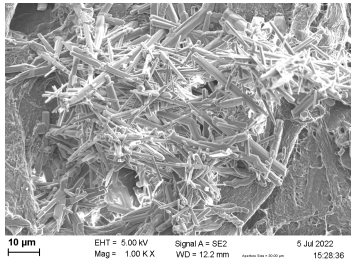

(i) 400 [ml/min], Time 2

Figure 3.17: Crystal morphology in function of the flow rate.

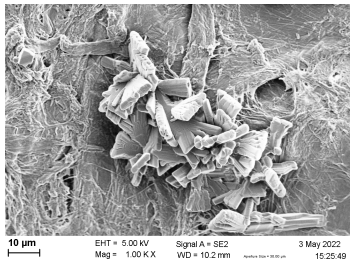

(a) 72 [turns/min], Time 0

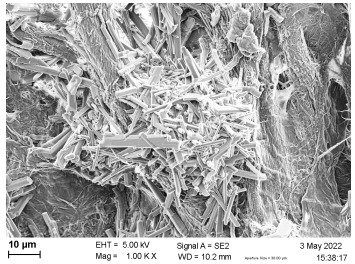

(b) 72 [turns/min], Time 1

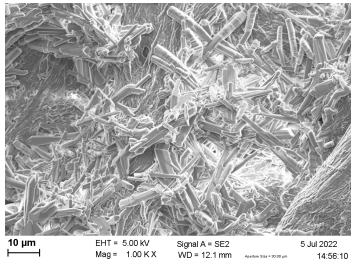

(c) 72 [turns/min], Time 2

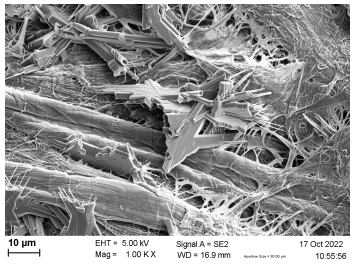

(d) 98 [turns/min], Time 0

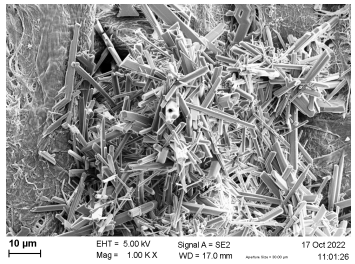

(e) 98 [turns/min], Time 1

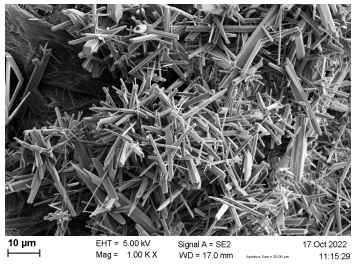

(f) 98 [turns/min], Time 2

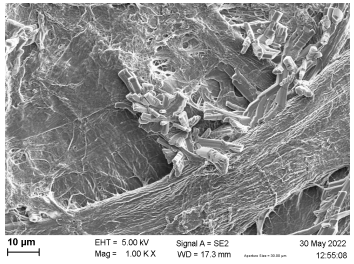

(g) 131 [turns/min], Time 0

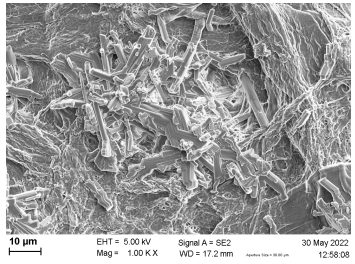

(h) 131 [turns/min], Time 1

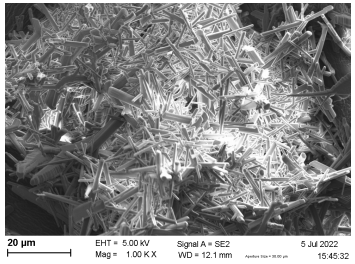

(i) 131 [turns/min], Time 2

Figure 3.18: Crystal morphology in function of the rotation speed.

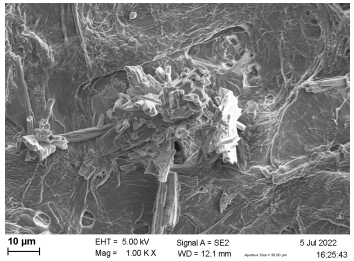

(a) 35 [°C], Time 0

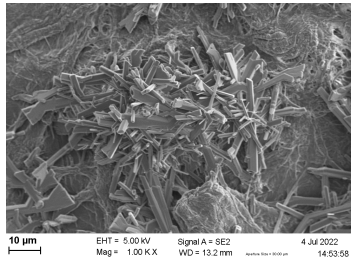

(b) 35 [°C], Time 1

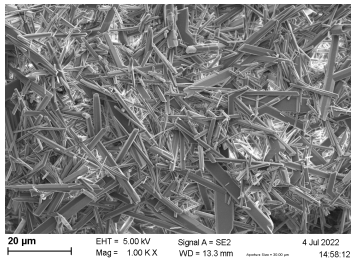

(c) 35 [°C], Time 2

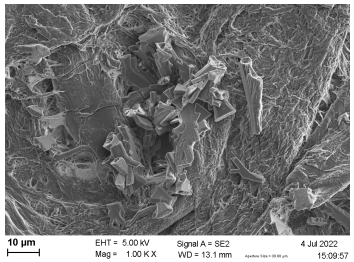

(d) 37.5 [°C], Time 0

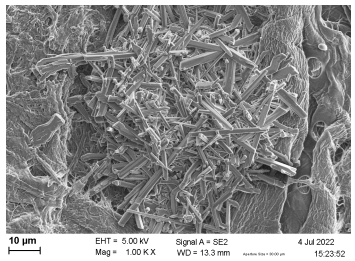

(e) 37.5 [°C], Time 1

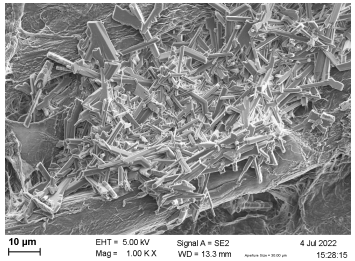

(f) 37.5 [°C], Time 2

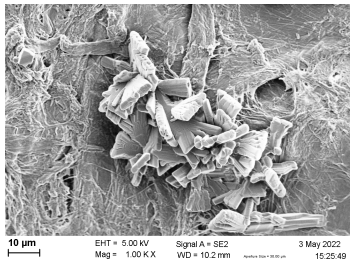

(g) 40 [°C], Time 0

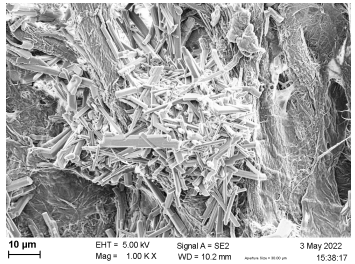

(h) 40 [°C], Time 1

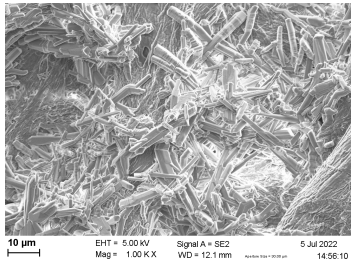

(i) 40 [°C], Time 2

Figure 3.19: Crystal morphology in function of the rotation speed.

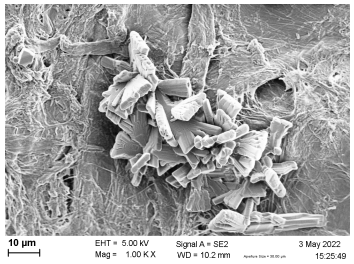

(a) 15 [mbar], Time 0

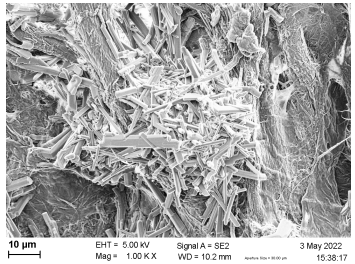

(b) 15 [mbar], Time 1

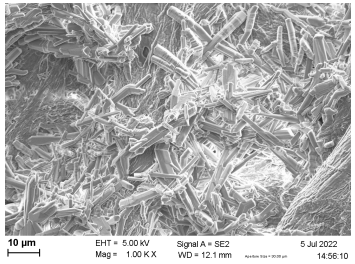

(c) 15 [mbar], Time 2

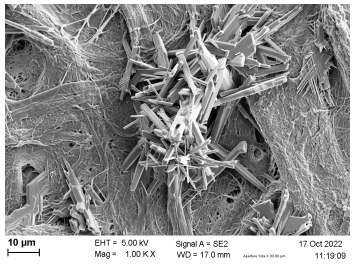

(d) 30 [mbar], Time 0

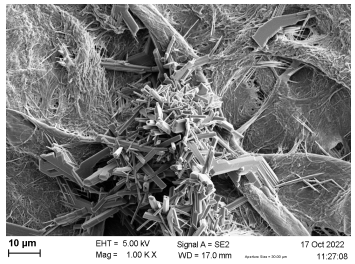

(e) 30 [mbar], Time 1

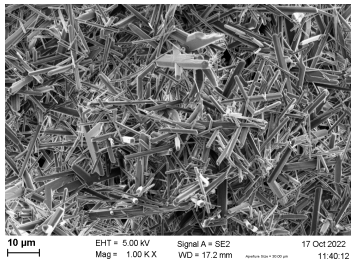

(f) 30 [mbar], Time 2

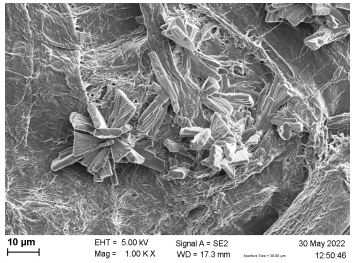

(g) 40 [mbar], Time 0

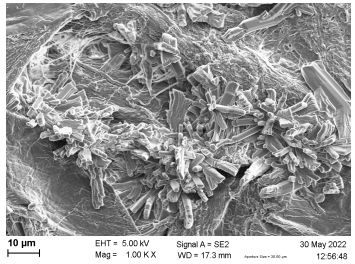

(h) 40 [mbar], Time 1

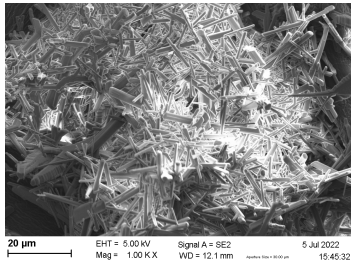

(i) 40 [mbar], Time 2

Figure 3.20: Crystal morphology in function of the vacuum level.

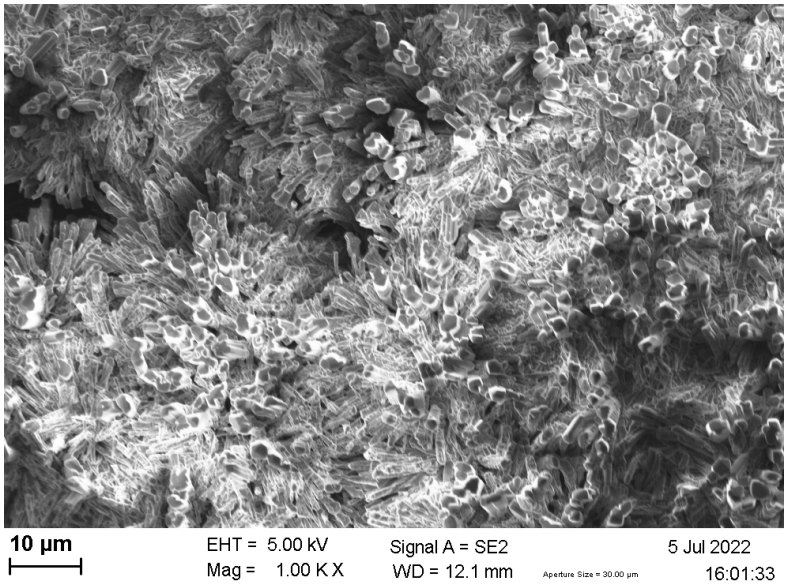

Figure 3.21: Experiment showing a different morphology.

The size distributions obtained with granulometry are shown in the figures 3.22, 3.23, 3.24 and 3.25. A reference experiment was left to crystallize for several additional hours to observe to what extent crystals could grow. The results of this experiment are shown in figure 3.26.

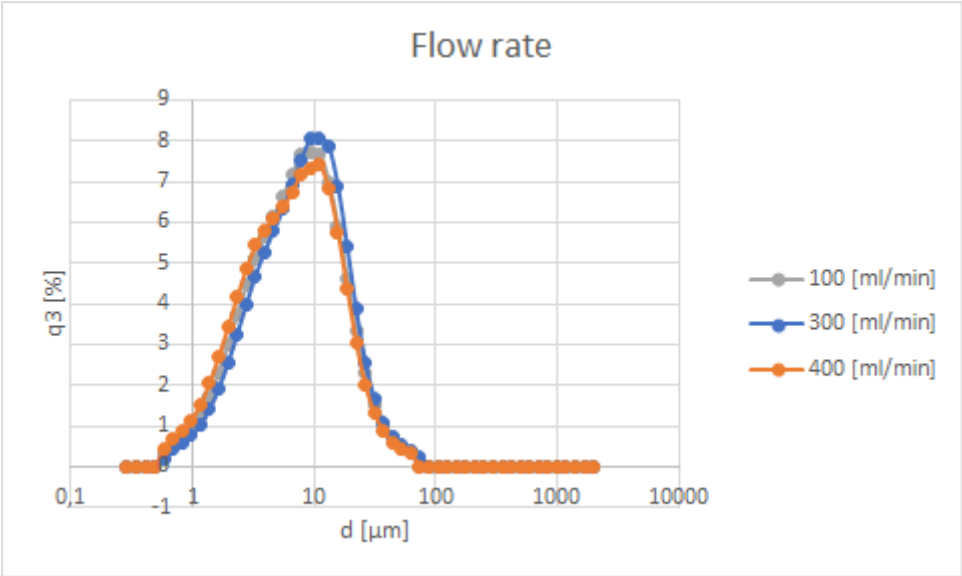

Figure 3.22: Size distribution in function of the flow rate in the system

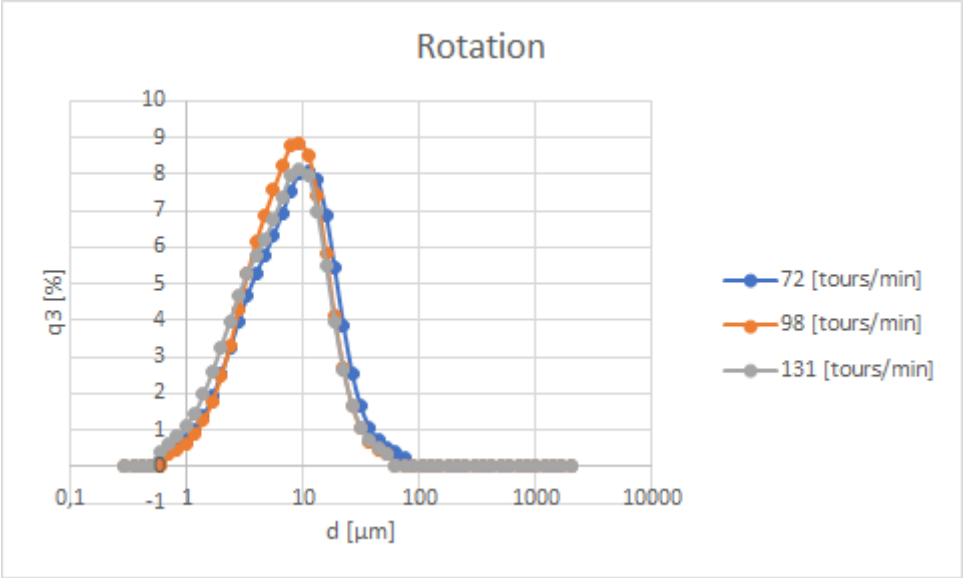

Figure 3.23: Size distribution in function of the rotation speed of the mixer in the crystallization body

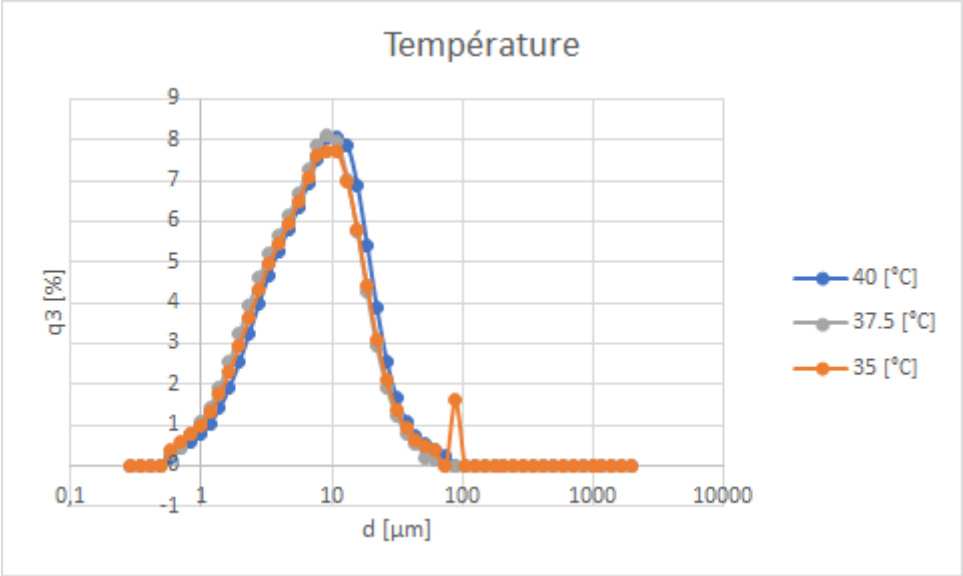

Figure 3.24: Size distribution in function of the temperature at the membrane inlet

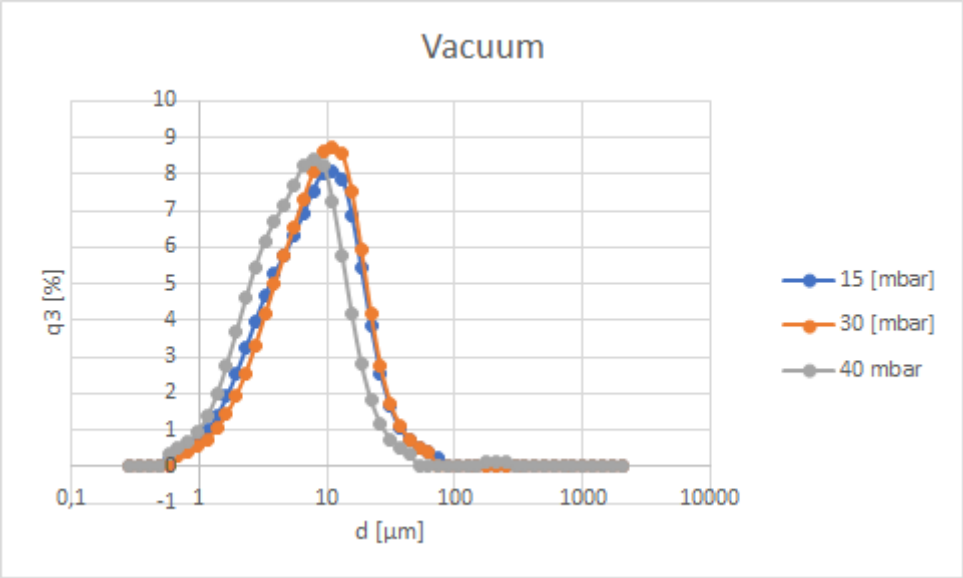

Figure 3.25: Size distribution in function of the level of vacuum at the outer side of the membrane

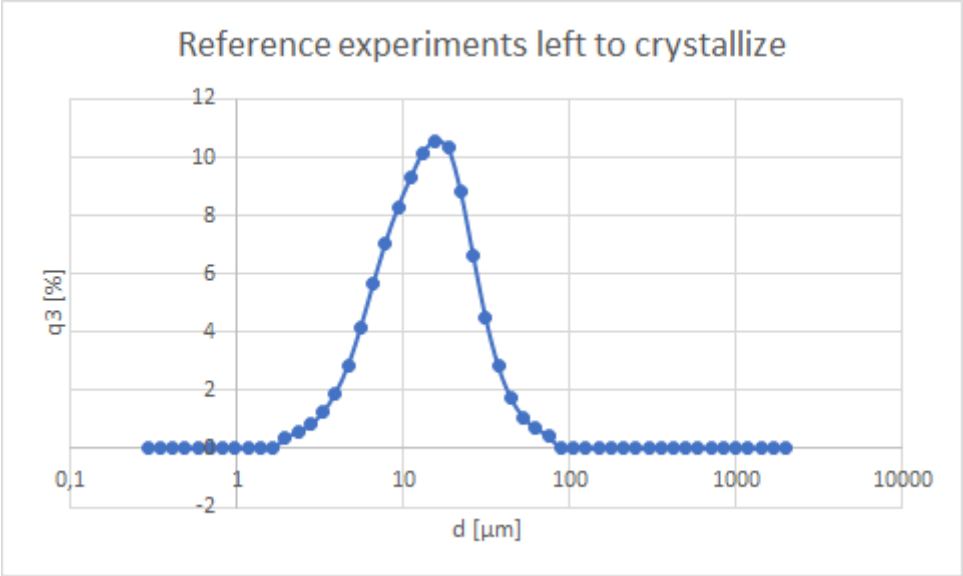

Figure 3.26: Size distribution of a reference experiment left to crystallize for one night

3.4 Crystal yield

The yields obtained for the different experiments are shown in the figures 3.27, 3.28, 3.29 and 3.30.

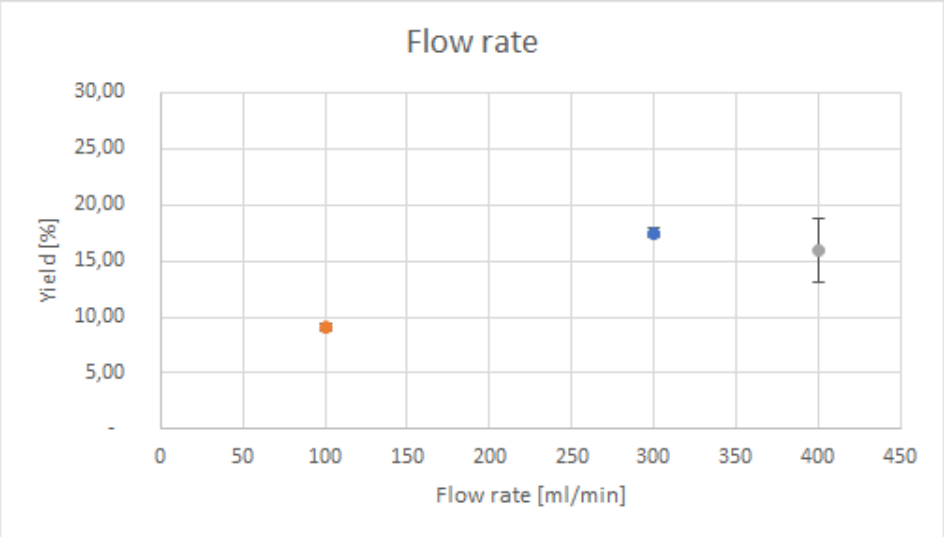

Figure 3.27: Yield in function of the flow rate in the system

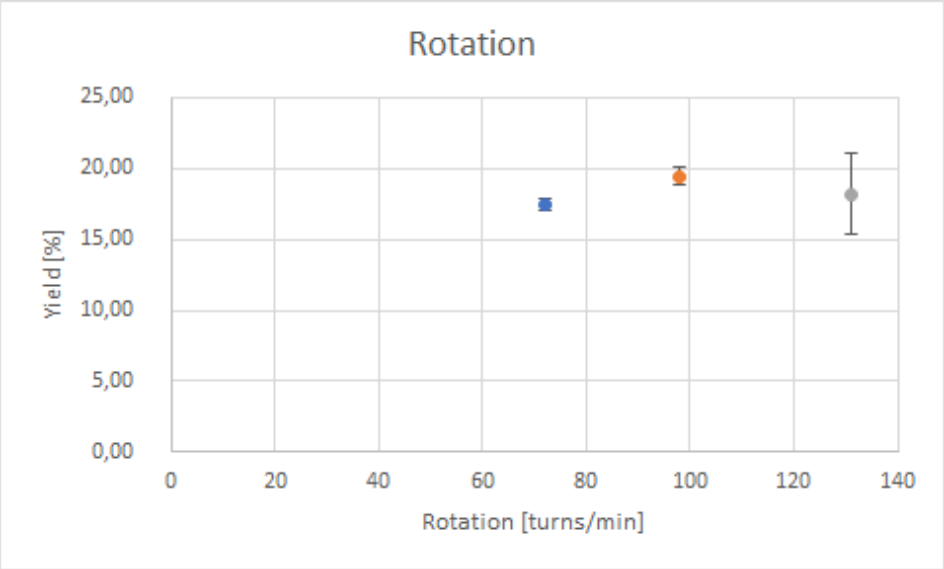

Figure 3.28: Yield in function of the rotation speed of the mixer in the crystallization body

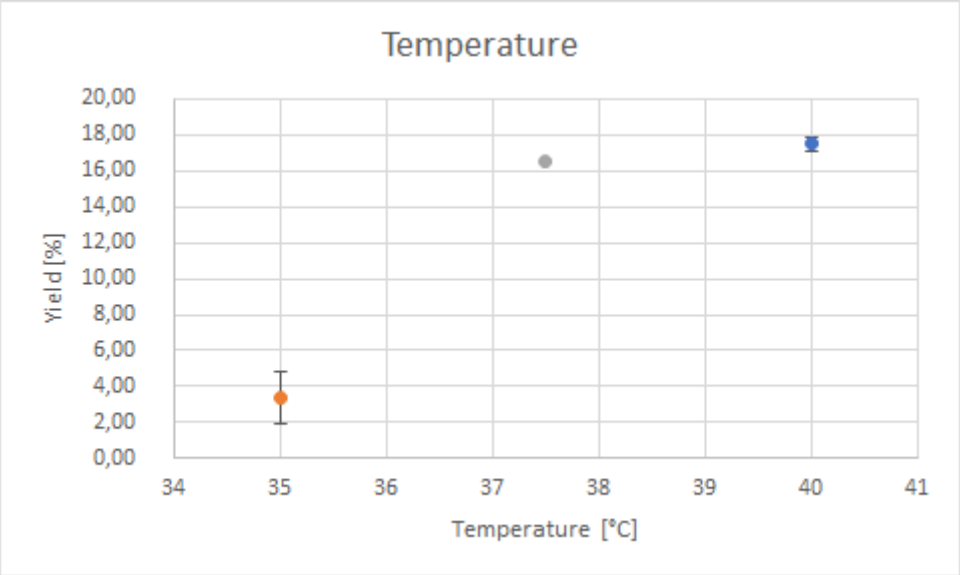

Figure 3.29: Yield in function of the temperature at the membrane inlet

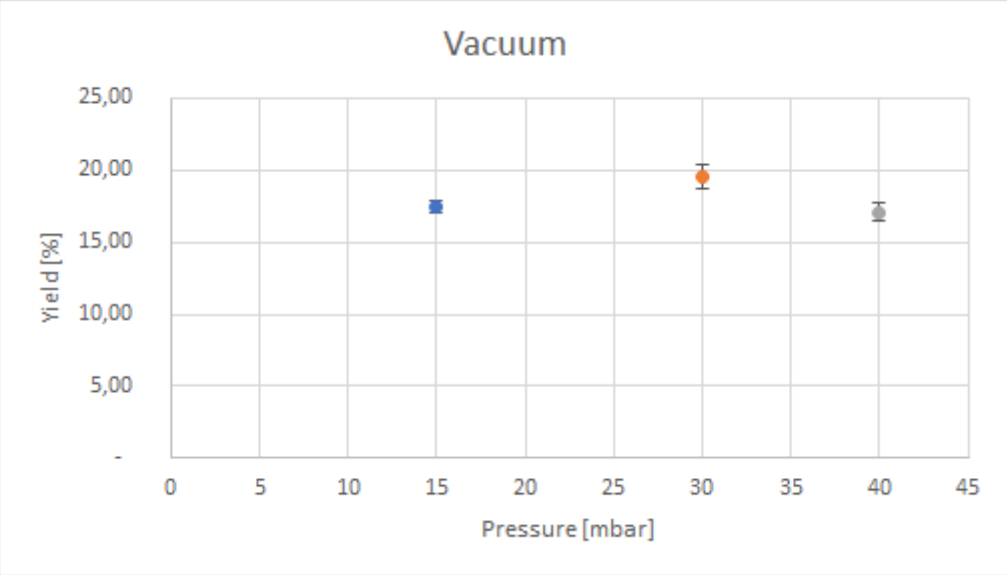

Figure 3.30: Yield in function of the level of vacuum at the outer side of the membrane

All the tested samples in XDR had their peaks at the same positions and only peaks of $NaHCO_3$ are observed. Therefore, only one result is presented in this section (some examples are shown in appendix C).

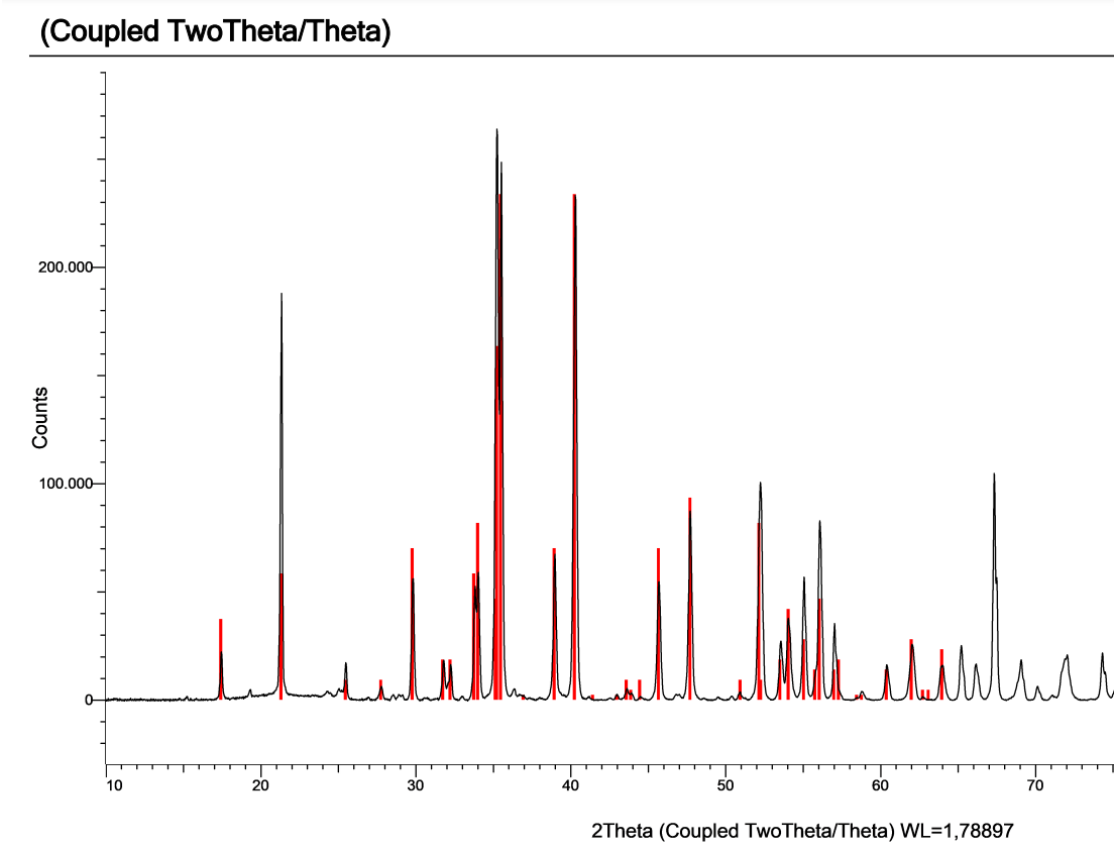

Figure 3.31: Results of the XRD with, in black, the tested sample and in red, the reference peaks recorded in the database for the Na_2CO_3 crystals.

Chapter 4

Discussion

In this chapter, the results presented in chapter 3 will be analyzed and discussed. The structure of this chapter will thus follow the one of chapter 3, to be known the induction time, the transfer coefficient, the size and shape of the crystals and the crystal yield.

Some propositions to improve results will also be proposed for some of these parameters.

4.1 Induction time

From figure 3.1, it can be seen that an increasing flow rate of the solution inside the membrane decreases the induction time as expected [19]. However, a slight increase occurs between a flow rate of 300 [ml/min] and 400 [ml/min]. Two explanations are possible.

First, a wetting of the membrane could occur. Indeed, the wetting of the membrane should decrease the evaporation rate and therefore decrease the induction time [5]. Nonetheless, the wetting of the membrane used is not supposed to occur before a flow rate of 500 [ml/min] (see appendix A). Two explanations are possible. The only acceptable assumption is that the membrane has been damaged by nucleation and/or growth of the crystals inside it.

Second, concentration polarization occurs on the membrane. Due to the evaporation of the solvent, the transfer coefficient decrease and so do the evaporation rate.

Further analysis are required to determine which of these two mechanism is responsible.

The rotation speed does not seem to have an impact on the induction time (see figure 3.2).

As for the flow rate, an increasing temperature seems to decrease the induction time as pictured in figure 3.3. Furthermore, an increasing pressure outside the membrane seems to increase the induction time 3.4. These two parameters affect indeed the evaporation rate [13].

It would be beneficial to conduct additional research on how the membrane's characteristics affect the induction time. Such thorough research could provide invaluable insights into the behaviour and performance of the membrane, and help to optimize its overall functionality and efficiency.

4.2 Transfer coefficient

As for the induction time, one can observe in figure 3.5 and 3.9 that both the flux and the overall transfer coefficient increase when the flow rate increase. The same remark can be done: a slight decrease is observed after 300 [ml/min] while the opposite was expected. This could be due to the wetting of the membrane.

One interesting observation is in the figures linked to the level of vacuum, an increasing pressure outside the membrane decreases the flux but increases the overall transfer coefficient (see figures 3.8 and 3.12). This result seems counter-intuitive but was actually expected. Studies conducted in the past have revealed that elevating the vacuum level leads to a higher transmembrane pressure gradient, which in turn enhances the probability of wetting [25].

Conversely, in the figures linked to the temperature, the flux increases with increasing feed temperature, but the overall transfer coefficient increases first to slightly decreases after 37.5 [°C]. In this case, temperature polarization is suspected to be the cause of the reduction in the overall transfer coefficient.

Finally, the rotation speed seems to first increase the flux and the overall transfer coefficient and then decrease them. The increase could be explained since this improved mixing and can help maintain a more uniform solute concentration throughout the solution, reducing concentration gradients that may hinder mass transfer to the membrane but no studies report such phenomena and it has thus still to be confirmed. The decrease in the flux and the overall transfer coefficient at higher rotation speed could be explained by the formation of a vortex when the level of the solution decreases in the crystallization tank. As discussed previously, such vortex would impact the residence time of the particles and impact the whole system.

4.3 Size and shape

4.3.1 Size

All size distribution shows the same profile, with slight variations. It is important to keep in mind here that all the first observations of the crystallization are done with the naked eye since the use of a turbidity probe was not possible as already discussed. This means that from one experiment to another, there could be some more time elapsed since the real start of crystallization before the observation is made and thus the size of the crystals could slightly vary. Therefore no conclusion taking this into account could be made in a safe way in order to identify a trend in the size distributions.

The small second peak that can be observed in figure 3.24 for the inlet temperature of 35[°C] is probably due to some agglomerates of crystals. In general, when dealing with samples that contain agglomerates, it is common practice to apply ultrasound to break them up. Nevertheless, in this case, some agglomerates have failed to undergo the expected splitting process despite being subjected to the ultrasound treatment.

The final observation that can be made is with the experiment that was left to crystallize during the night. It shows a similar size distribution profile, shifted of about five [μm] to the right, as the other experiments. As already said, it is expected to have an increasing coefficient of variation and mean diameter if the time of crystallization increases [24]. This is indeed the case here (due to the logarithmic scale, the coefficient of variation does increase).

Since the membrane composition could also lead to higher uniformity it would be great to explore this in further study. As well, seeding influence the size distribution of the crystals by reducing the probability of small crystals to and could also be study.

4.3.2 Shape

The figures 3.13, 3.14, 3.15 and 3.16 show that all the experiments crystallized with a degree of supersaturation between 35% and 45%. According to figure 2.3, at such degree of supersaturation, the morphology of the crystals should be dendrites.

This is indeed what can be observed in figures 3.17, 3.19, 3.18 and 3.20. However, the first crystals (time 0) show some intergrowths between flat twins, which should occur at a slightly higher degree of supersaturation. This can in fact be easily explained. The degree of supersaturation is computed based on the titration made at the end of the experiments. Nevertheless, this degree decreased as concentration decreases too, which is exactly what happens when crystallization occurs.

One could observe in the figures obtained with the SEM that, even if their

morphology seems the same, their size varies slightly through experiments, but as said in the previous subsection, this is probably due to the fact that the first observations of the crystallization are done with the naked eye. Due to the same reason, no trend can properly be identified in the degree of supersaturation which is directly related to the concentration that varies with the duration of crystallization.

Indeed, when crystallization starts, the concentration (and so the degree of supersaturation) decreases. There are therefore no exact certitudes about the time between the beginning and the stop of the crystallization and this could be the cause of the observed variations in the degree of supersaturation.

Figure 3.21 shows a SEM picture of a sample that has given crystals with different morphology. This particular sample was obtained from a series of experiments that were conducted multiple times. However, it is worth noting that the outcome presented here was obtained only once, making it a unique observation (the other results being similar to the other experiment). The degree of supersaturation computed for this sample was about 60%. It seems that the crystallization started later for this specific sample. So far, no valid explanation can be done.

4.4 Crystal yield

As said previously, studies showed that the crystallization yield increases with an increasing feed temperature [6]. One can see in figure 3.29 that is indeed the case for the crystallization of $NaHCO_3$, ranging from about 4% at 35[°C] to almost 18% at 40[°C] after ten minutes of crystallization.

An experiment was carried out wherein the solution was left to crystallize for a substantial period of time within the tank, specifically overnight, in order to achieve the maximum possible growth of crystals. This experiment showed a crystal yield of 61%. This is far from the 80% in the conventional crystallization but the scale of the process may be the reason for such difference [24].

In addition to the temperature, a higher flow rate seems to also increase the yield as shown in figure 3.27. Indeed, the flow rate may help to reduce the fouling on the membrane surface by preventing the accumulation of crystals which would inhibit crystallization and decrease crystal yield.

Finally, nor the rotation speed, nor the vacuum level showed a significant impact on the crystal yield (see figures 3.28 and 3.30).

As previously stated, the implementation of seeding - a process which involves the introduction of small crystal fragments - has the potential to significantly enhance crystal yield rates. The merits of this approach make it an avenue worthy of further exploration and study.

Chapter 5

Conclusion

In conclusion, the conducted experimental study provides valuable insights into the crystallization process of $NaHCO_3$ and its relationship with various operational parameters.

The induction time, a critical aspect of crystallization, exhibits a clear trend with flow rate, demonstrating a decrease with increasing flow rate up to 400 [ml/min], albeit with a slight unexpected drop between 300 [ml/min] and 400 [ml/min]. Possible explanations include membrane wetting or concentration polarization, the latter resulting from solvent evaporation. Further investigations are needed to ascertain the dominant mechanism responsible for this behaviour.

Temperature and external pressure appear influential, affecting the evaporation rate and consequently, the induction time. Higher temperatures seem to decrease induction time, whereas elevated pressure outside the membrane lengthens it. Moreover, transfer coefficient analysis reveals a correlation with flow rate, temperature, and vacuum level. Surprisingly, an increase in external pressure enhances the overall transfer coefficient despite decreasing the flux, a counterintuitive observation attributed to transmembrane pressure gradients and potential wetting.

In the context of crystal size and shape, the experimental data indicate consistent profiles for size distributions with slight variations, linked to the inherent variability in crystallization duration. Crystal morphology, predominantly dendritic, corresponds to the calculated degree of supersaturation. The influence of membrane composition and seeding on size distribution requires further exploration.

In terms of crystal yield, temperature and flow rate emerge as significant factors, with higher values of both leading to increased yield. Notably, rotation speed and vacuum level exhibited minor impacts on yield. The prospect of seeding as a yield enhancement strategy is promising and merits additional investigation.

In sum, this comprehensive investigation illuminates the intricate interplay of operational parameters on $NaHCO_3$ crystallization. The findings underscore the need for further research to elucidate underlying mechanisms, optimize membrane

characteristics, and explore innovative approaches such as seeding for yield enhancement, or introducing contaminants in order to study its impact on the purity of the crystals. This study lays a foundation for improved understanding and control of crystallization processes.

Bibliography

[1] Catherine Charcosset et al. "Coupling between Membrane Processes and Crystallization Operations". In: *Industrial and Engineering Chemistry Research* 49.12 (June 2010), pp. 5489–5495. ISSN: 08885885. DOI: 10.1021/IE901824X. URL: https://pubs.acs.org/doi/abs/10.1021/ie901824x.

[2] Peter Crafts. "The Role of Solubility Modeling and Crystallization in the Design of Active Pharmaceutical Ingredients". In: *Computer Aided Chemical Engineering* 23 (Jan. 2007), pp. 23–85. ISSN: 1570-7946. DOI: 10.1016/S1570-7946(07)80005-8.

[3] "Crystallisation, 4th Edition By J. W. Mullin. 2001. Butterworth Heinemann: Oxford, UK. ISBN 075-064-833-3." In: *Organic Process Research & Development* 6.2 (Mar. 2001), pp. 201–202. ISSN: 1083-6160. DOI: 10.1021/OP0101005. URL: https://pubs.acs.org/doi/abs/10.1021/op0101005.

[4] Zhaoliang Cui et al. "Testing of three different PVDF membranes in membrane assisted-crystallization process: Influence of membrane structural-properties on process performance". In: *Desalination* 440 (Aug. 2018), pp. 68–77. ISSN: 0011-9164. DOI: 10.1016/J.DESAL.2017.12.038.

[5] Gianluca Di Profio et al. "Controlling polymorphism with membrane-based crystallizers: Application to form i and II of paracetamol". In: *Chemistry of Materials* 19.10 (May 2007), pp. 2386–2388. ISSN: 08974756. DOI: 10.1021/CM0701005/ASSET/IMAGES/CM0701005.SOCIAL.JPEG{_}V03. URL: https://pubs.acs.org/doi/abs/10.1021/cm0701005.

[6] Felinia Edwie and Tai Shung Chung. "Development of simultaneous membrane distillation–crystallization (SMDC) technology for treatment of saturated brine". In: *Chemical Engineering Science* 98 (July 2013), pp. 160–172. ISSN: 0009-2509. DOI: 10.1016/J.CES.2013.05.008.

[7] John Haleblian and Walter McCrone. "Pharmaceutical Applications of Polymorphism". In: *Journal of Pharmaceutical Sciences* 58.8 (Aug. 1969), pp. 911–929. ISSN: 0022-3549. DOI: 10.1002/JPS.2600580802.

[8] Tung A. Hoang. "Mechanisms of scale formation and inhibition". In: *Water-Formed Deposits: Fundamentals and Mitigation Strategies* (Jan. 2022), pp. 13–47. DOI: 10.1016/B978-0-12-822896-8.00031-5.

[9] Shifeng Jiang, Yuande Zhang, and Zhibao Li. "A new industrial process of NaHCO3 and its crystallization kinetics by using the common ion effect of Na2CO3". In: *Chemical Engineering Journal* 360 (Mar. 2019), pp. 740–749. ISSN: 1385-8947. DOI: 10.1016/J.CEJ.2018.12.028.

[10] Xiaobin Jiang et al. "Membrane Crystallization for Process Intensification and Control: A Review". In: *Engineering* 7.1 (Jan. 2021), pp. 50–62. ISSN: 2095-8099. DOI: 10.1016/J.ENG.2020.06.024.

[11] Kohsaku Kawakami et al. "Impact of degree of supersaturation on the dissolution and oral absorption behaviors of griseofulvin amorphous solid dispersions". In: *Journal of Drug Delivery Science and Technology* 56 (Apr. 2020), p. 101172. ISSN: 1773-2247. DOI: 10.1016/J.JDDST.2019.101172.

[12] Junghyun Kim, Jungwon Kim, and Seungkwan Hong. "Recovery of water and minerals from shale gas produced water by membrane distillation crystallization". In: *Water Research* 129 (Feb. 2018), pp. 447–459. ISSN: 0043-1354. DOI: 10.1016/J.WATRES.2017.11.017.

[13] Patricia Luis. "Membrane contactors". In: *Fundamental Modeling of Membrane Systems: Membrane and Process Performance* (Jan. 2018), pp. 153–208. DOI: 10.1016/B978-0-12-813483-2.00005-8.

[14] Francesca Macedonio and Enrico Drioli. "Hydrophobic membranes for salts recovery from desalination plants". In: *New pub: Balaban* 18.1-3 (2012), pp. 224–234. ISSN: 19443986. DOI: 10.5004/DWT.2010.1775. URL: https://www.tandfonline.com/doi/abs/10.5004/dwt.2010.1775.

[15] Francesca Macedonio et al. "Bi2Se3-assisted membrane crystallization". In: *Materials Horizons* 5.5 (Sept. 2018), pp. 912–919. ISSN: 20516355. DOI: 10.1039/C8MH00612A.

[16] Allan S Myerson, Deniz Erdemir, and Alfred Y Lee Frontmatter. "Handbook of Industrial Crystallization Edited Handbook of Industrial Crystallization". In: *Separations Science and Technology* (2008). DOI: 10.1017/9781139026949. URL: www.cambridge.org.

[17] *Particles, scaling and biofouling.* URL: https://www.lenntech.com/particles-scaling-biofouling.htm.

[18] Maria Luisa Perrotta et al. “Graphene stimulates the nucleation and growth rate of NaCl crystals from hypersaline solution via membrane crystallization”. In: *Environmental Science: Water Research & Technology* 6.6 (June 2020), pp. 1723–1736. ISSN: 2053-1419. DOI: 10.1039/C9EW01124B. URL: https://pubs.rsc.org/en/content/articlehtml/2020/ew/c9ew01124b%20https://pubs.rsc.org/en/content/articlelanding/2020/ew/c9ew01124b.

[19] C. A. Quist-Jensen, F. Macedonio, and E. Drioli. “Membrane crystallization for salts recovery from brine—an experimental and theoretical analysis”. In: *New pub: Balaban* 57.16 (Apr. 2015), pp. 7593–7603. ISSN: 19443986. DOI: 10.1080/19443994.2015.1030110. URL: https://www.tandfonline.com/doi/abs/10.1080/19443994.2015.1030110.

[20] Cejna Anna Quist-Jensen et al. “Reclamation of sodium sulfate from industrial wastewater by using membrane distillation and membrane crystallization”. In: *Desalination* 401 (Jan. 2017), pp. 112–119. ISSN: 0011-9164. DOI: 10.1016/J.DESAL.2016.05.007.

[21] Mohammad Rezaei et al. “Wetting phenomena in membrane distillation: Mechanisms, reversal, and prevention”. In: *Water Research* 139 (Aug. 2018), pp. 329–352. ISSN: 0043-1354. DOI: 10.1016/J.WATRES.2018.03.058.

[22] M. Sarbar et al. “The activity and osmotic coefficients of aqueous sodium bicarbonate solutions”. In: *The Journal of Chemical Thermodynamics* 14.10 (Oct. 1982), pp. 967–976. ISSN: 0021-9614. DOI: 10.1016/0021-9614(82)90006-4.

[23] Yonghyun Shin and Jinsik Sohn. “Mechanisms for scale formation in simultaneous membrane distillation crystallization: Effect of flow rate”. In: *Journal of Industrial and Engineering Chemistry* 35 (Mar. 2016), pp. 318–324. ISSN: 1226-086X. DOI: 10.1016/J.JIEC.2016.01.009.

[24] Marie Charlotte Sparenberg et al. “Crystallization control via membrane distillation-crystallization: A review”. In: *Desalination* 519 (Dec. 2021), p. 115315. ISSN: 0011-9164. DOI: 10.1016/J.DESAL.2021.115315.

[25] Marie Charlotte Sparenberg et al. “Experimental mass transfer comparison between vacuum and direct contact membrane distillation for the concentration of carbonate solutions”. In: *Separation and Purification Technology* 275 (Nov. 2021), p. 119193. ISSN: 1383-5866. DOI: 10.1016/J.SEPPUR.2021.119193.

[26] Sreepriya Vedantam and Vivek V. Ranade. “Crystallization: Key thermodynamic, kinetic and hydrodynamic aspects”. In: *Sadhana - Academy Proceedings in Engineering Sciences* 38.6 (Dec. 2013), pp. 1287–1337. ISSN: 02562499. DOI: 10.1007/S12046-013-0195-4/METRICS. URL: https://link.springer.com/article/10.1007/s12046-013-0195-4.

[27] Zhongsen Yan et al. “Integration of seeding- and heating-induced crystallization with membrane distillation for membrane gypsum scaling and wetting control”. In: *Desalination* 511 (Sept. 2021), p. 115115. ISSN: 0011-9164. DOI: 10.1016/J.DESAL.2021.115115.

Appendix A

Membrane characteristics

3M | Liqui-Cel™ Membrane Contactors

3M™ Liqui-Cel™ MM-1×5.5 Series Membrane Contactor

Typical Properties

Membrane Characteristics	
Cartridge Configuration	Parallel Flow. Lumenside Liquid Flow.
Liquid Flow Guidelines	< 500 ml/min
Membrane Type	X50 Fiber
Membrane/Potting Material	Polypropylene/Polyurethane
Priming Volume (approximate)	
Shellside	25 ml
Lumenside	16 ml

Pressure Guidelines*	
Maximum Lumenside LIQUID Working Temperature/ Pressure	5-20°C, 4.1 barg (41-68°F, 60 psig) 40°C, 2.1 barg (104°F, 30 psig)

* Note: Liquid pressure should always exceed gas pressure.

Housing Characteristics	
Material	Polycarbonate
Flange Connections	
Shellside (gas/vacuum)	Standard Female Luer Lock with Polycarbonate adaptors to ¼ inch Hosebarb
Lumenside (wetted surface)	¼ inch FNPT

Weight (approximate)	
Dry	47 grams

Regulatory

Complies with the limits as set by RoHS Directive 2011/65/EU Annex II; recasting 2002/95/EC. Constructed of FDA CFR title 21 compliant materials for wetted parts only at ambient temperatures.

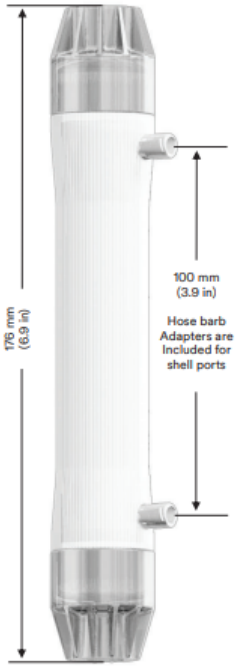

All dimensions are nominal values. See full housing drawing on 3M.com/Liqui-Cel for additional details.

3M™ Liqui-Cel™ MM-1×5.5 Series Membrane Contactor

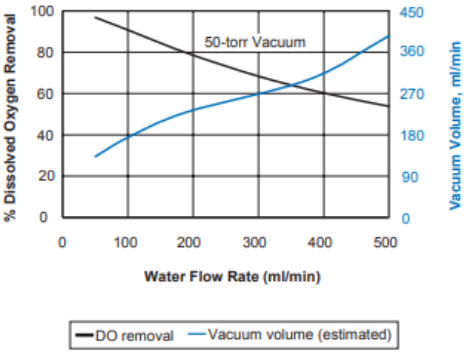

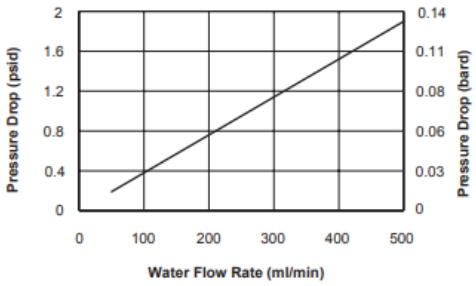

Curves represent nominal values, generated using water on the Lumenside at 20°C with 50 torr of vacuum drawn on both Shellside ports. The estimated vacuum volume guideline is based on a flow rate at 20°C, 50 Torr. Characteristics may change under different operating conditions.

Certified System ™
ISO 9001

3M

Appendix B

Sodium hydrogen carbonate characteristics

Product Specification

Material	27778.360
Material description	Sodium hydrogen carbonate
Grade	AnalaR NORMAPUR Reag. Ph.Eur.
CAS Number	144-55-8
Molecular formula	$NaHCO_3$
Molecular mass	84.01

Characteristics	Specifications
Assay (calculated on dried substance)	99.7 - 100.3 %
Appearance of solution	Passes test Ph.Eur.
Carbonates	Passes test Ph.Eur.
Identification A	Passes test Ph.Eur.
Identification B	Passes test Ph.Eur.
Identification (Na)	Passes test Ph.Eur.
Solution S	Passes test Ph.Eur.
Heavy metals (as Pb)	≤ 5 ppm
Insolubility in water	≤ 0.015 %
Loss on drying	≤ 0.2 %
Reducing substances (as I)	≤ 65 ppm
Total N (Nitrogen)	≤ 5 ppm
Total S (as SO_4)	≤ 30 ppm
Cl (Chloride)	≤ 50 ppm
NH_4 (Ammonium)	≤ 5 ppm
PO_4 (Phosphate)	≤ 10 ppm
SO_4 (Sulphate)	≤ 20 ppm
As (Arsenic)	≤ 2 ppm
Ca (Calcium)	≤ 100 ppm
Cu (Copper)	≤ 2 ppm
Fe (Iron)	≤ 5 ppm
K (Potassium)	≤ 50 ppm
Mg (Magnesium)	≤ 50 ppm
Pb (Lead)	≤ 5 ppm
Conforms to Reag. Ph.Eur.	Passes test

Appendix C

XRD

In the following figures, the black line represents the results of the $NaHCO_3$ powder used to prepare the solution, and in colour are the results from the experiments.

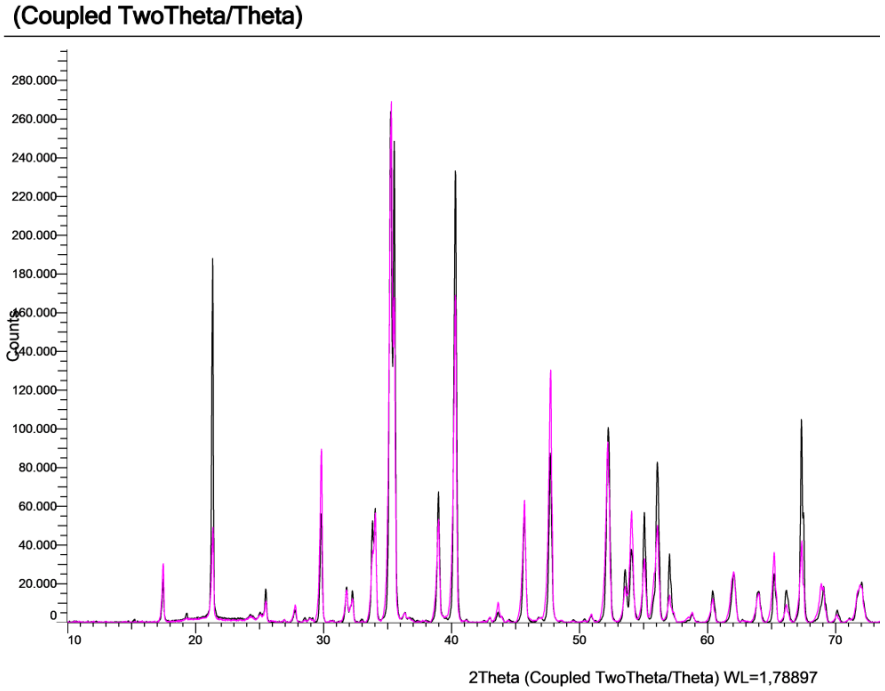

(Coupled TwoTheta/Theta)

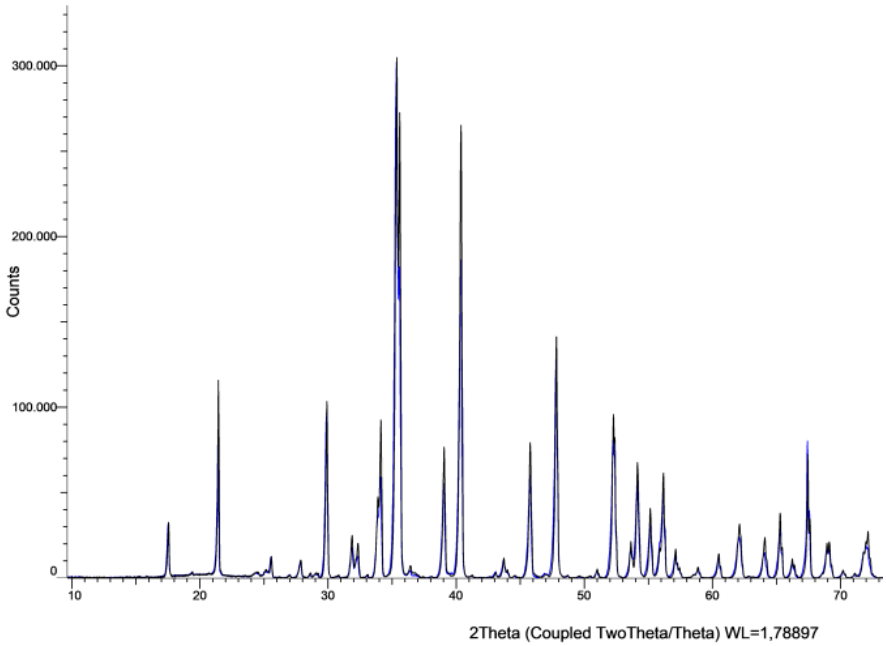

(Coupled TwoTheta/Theta)

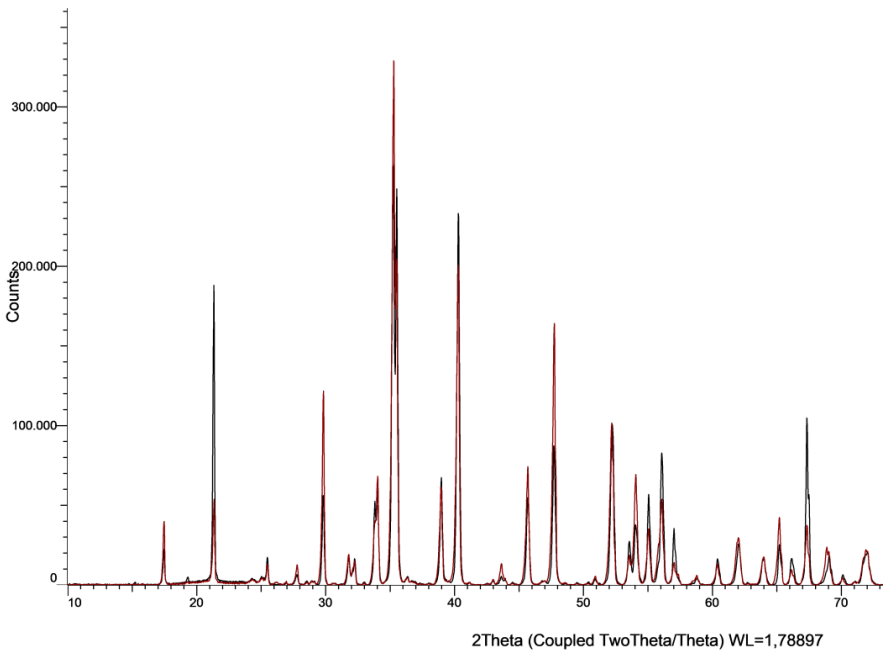

(Coupled TwoTheta/Theta)

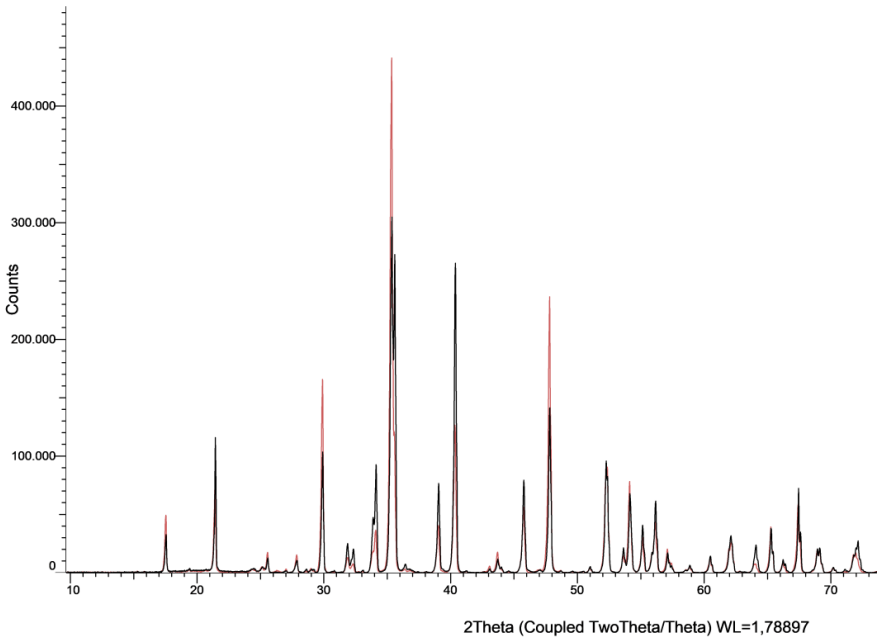

UNIVERSITÉ CATHOLIQUE DE LOUVAIN
École polytechnique de Louvain
Rue Archimède, 1 bte L6.11.01, 1348 Louvain-la-Neuve, Belgique | **www.uclouvain.be/epl**